Received: 28 May 2024 | Revised: 17 September 2024 | Accepted: 27 September 2024

DOI: 10.1002/eqe.4248

RESEARCH ARTICLE

WILEY

Simulating column splice fracture and post-fracture response for seismic assessment of steel moment frames

Aditya Jhunjhunwala | **Arka Maity** | **Amit Kanvinde**

Department of Civil and Environmental Engineering, University of California, Davis, California, USA

Correspondence
Aditya Jhunjhunwala, Department of Civil and Environmental Engineering, University of California, Davis, CA, USA.
Email: arjhunjhunwala@ucdavis.edu

Funding information
Pacific Earthquake Engineering Research Center, University of California Berkeley, Grant/Award Number: 1158-NCTRVI; National Science Foundation, Grant/Award Number: 2129445

Abstract

Mitigating fracture in welded column splices is an important challenge for the safety of existing steel moment-resisting frames. While models to predict splice fracture have recently been developed, suitable approaches are not available to simulate the response of frames after splice fracture. Motivated by this, a two-dimensional displacement-based fiber element construct, termed the Splice Fracture Element (SFE), is presented. The SFE includes numerous features: (1) representation of the loss of strength in any fiber at a critical stress determined from fracture mechanics, (2) the ability to simulate the loss of shear strength of the cross-section when the entire section is severed – a phenomenon not readily simulated in conventional fiber elements, and (3) the ability to track the kinematics of the severed parts of the column to represent transfer of compressive stresses on contact. This formulation is implemented into an open-source software (OpenSees) and applied to conduct Nonlinear Response History Analysis (NLRHA) of two demonstration problems, including a 1-story frame and a 20-story frame. Benchmark simulations that do not simulate splice fracture or represent it without the loss of shear strength are also conducted. The results indicate that the SFE element can successfully simulate the key phenomena associated with splice fracture and post-fracture response.

KEYWORDS
column splices, frame elements, fracture, steel moment frames

1 | INTRODUCTION AND MOTIVATION

Steel Moment Frames (SMFs) are commonly used as lateral load resisting systems in seismic regions of the United States and elsewhere. While modern SMFs are known for their architectural versatility and ductility, the performance of SMFs constructed in the United States in the 1960–1994 era has come under recent scrutiny.[1] These frames (termed "pre-Northridge" frames) were constructed prior to major code revisions that followed the 1994 Northridge earthquake, during which numerous brittle fractures were observed in welded beam-to-column connections.[2,3] These pre-Northridge frames contain deficient connection details as well as low-toughness base and weld materials that have since been disallowed.[4]

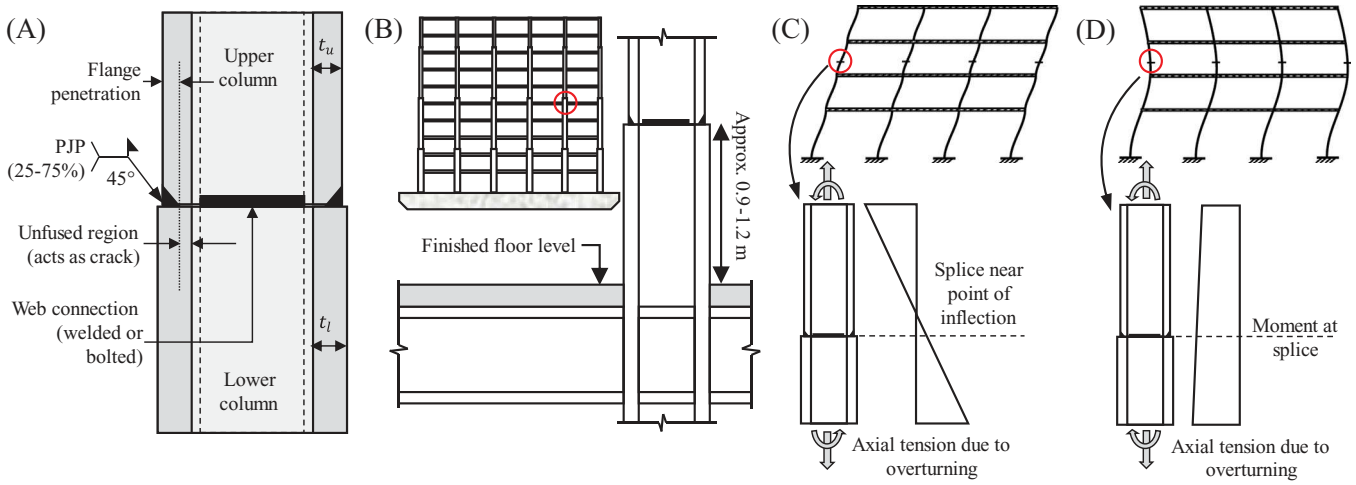

FIGURE 1 (A) Typical pre-Northridge splice detail (B) Location of splice in frame (C) First-mode response of building and bending of column in double curvature (D) Higher mode response of building and bending of column in single curvature.

Of particular concern in these frames are welded column splice connections that are usually provided near the mid-story height. Numerous studies, both academic, e.g., Galasso et al.,[5] Shaw et al.,[6] Shen et al.,[7] and Song et al.,[8] as well as professional,[9] suggest that welded column splices may be highly susceptible to fracture. Figure 1A illustrates a typical pre-Northridge column splice connection detail, and Figure 1B illustrates its location within a moment frame.

Referring to Figure 1A, these connections were typically constructed using Partial Joint Penetration (PJP) welds with flange penetrations (i.e., ratio of weld size to flange thickness) in the range of 25–75%. This practice is attributed to the assumption of first-mode response of the building (see Figure 1C), which implies that flange stresses near the mid-height of the story are low, owing to the presence of an inflection point near this location. This results in an unfused region (which is 25–75% of the flange) creating a notch condition similar to a sharp crack. Additionally, both base and weld filler materials used in these connections may have unacceptably low Charpy V-Notch impact energies in the range of 6.8–13.6 J at 21.1°C (5-10 ft-lb at 70°F).[10–12] In contrast, "post-Northridge" welded splices are constructed using notch-tough materials (with CVN energies mandated to be 54.2 J at 21.1°C, i.e., 40 ft-lb at 70°F) and high penetration PJP welds (i.e., flange penetration greater than 85%) with reinforcing fillet welds or Complete Joint Penetration (CJP) welds designed to preclude fracture.[4,13] The combination of low-toughness materials and the large unfused regions in pre-Northridge splices imply that these splices are highly vulnerable to fracture, at flange tensile stresses in the range of 70–140 MPa (10-20 ksi) depending on the configuration of the splice.[13] These stress capacities are significantly lower than anticipated demands in these splices (see Galasso et al.[5]), that arise from a combination of: (1) higher mode response resulting in single curvature bending of the column – see Figure 1D, and (2) overturning effects leading to net tension in the column. These effects were typically disregarded in the original design of these splices.

Nonlinear Response History Analysis (NLRHA) conducted in a probabilistic framework, by Galasso et al.[5] and Song et al.,[8] estimates that for many buildings on the West Coast of the United States, a convolution of these flange stresses with the local seismic hazard results in unacceptably high probabilities of splice fracture (return periods for fracture in the range of 75–400 years in four-story frames and 87–156 years in 20-story frames). It is important to acknowledge that column splice fractures have not been documented in post-Northridge reconnaissance studies.[2,3] No efforts to specially discover or document splice fractures were conducted – with the result that no splice fractures were found. However, for further context, it is also relevant to note that even the beam-column connection fractures (which became the major focus of post-Northridge connection studies[14,15]) were discovered somewhat serendipitously.[16] Due to these various reasons, the vulnerability of pre-Northridge splices has come to light relatively only recently, mainly through NLRHA and fracture mechanics simulations conducted as part of research studies[5–8] as well as building evaluation studies in the professional practice.[9] Moreover, similar welded box column splices were observed to fracture during the 1995 Kobe earthquake[17] corroborating the results of the analytical studies that indicate these splices to be vulnerable. Ultimately, the consequence is that a large majority of these splices are not retrofitted. The decision to retrofit these splices is a high-stakes decision because leaving them in place without retrofit requires accepting risk of fracture, whereas retrofitting them is costly and highly disruptive to building operations.[18]

In response to these issues, the United States government (National Institute of Standards and Technology) recently published a long-term research plan to address the safety of pre-Northridge SMFs with a major focus on column splices.[19] The ultimate goal of this research is to develop a toolset for predicting and simulating splice fracture, such that the trade-offs regarding retrofit may be evaluated rigorously within a probabilistic, performance-based framework. Development of approaches for accurately predicting splice fracture is a key component of this toolset, and various efforts have been made in this direction. These include the development of fracture mechanics-based models, and their implementation in software tools[20] as well as closed form equations.[13,21] However, the focus in these tools is entirely on the prediction of splice fracture (or its probability), but not the simulation of the connection (or the frame) after splice fracture. As a result, performance-based assessments of buildings using these tools (such as Galasso et al.[5]) usually assume splice fracture (specifically, the fracture of one flange within the splice) to be the endpoint of simulation, i.e., analogous to collapse. This is possibly a conservative assumption because fracture of a single flange in the splice may not result in unstable propagation through the entire splice, or to other splices or to system collapse, which depends on other factors including: (1) post-fracture response of the splice connection itself, (2) interaction of this response with the frame, or redistribution of forces within the frame, and (3) characteristics of the ground motion.

The precise manner of building response after the initiation of splice fracture is unknown due to the lack of research addressing this issue directly (e.g., there are no shake table tests with splice fracture). Insights regarding such response may be drawn from various sources, but they are largely speculative; specifically: (1) field observations after the 1995 Kobe earthquake noted that the column fracture (which may be expected to influence building response similarly) did not lead to building collapse, (2) component scale experiments on splices is inconclusive in this regard, e.g., one experiment by Bruneau and Mahin[22] shows complete breakage of the splice after initiation, whereas more recent experiments by Shaw et al.[6] albeit with larger weld penetration and tougher materials, show propagation through only one flange and the web, but not the other flange. None of these experiments feature axial loading in the splices, and all experiments were loaded in a quasi-static way, rather than dynamically. In the absence of shake table data which directly interrogates frame response after splice fracture, NLRHA simulations become necessary. However, effective tools to simulate the post-fracture response of the splice and its interaction with global frame response within NLRHA are not available either. This may be attributed to the highly complex nature of the post-fracture response of splices, with phenomena such as: (1) coupling between tension or flexure induced fracture and loss of shear continuity provided by the splice, which occurs when the entire splice is severed, (2) loss of contact between the columns, and seating or bouncing of the upper column segment on the lower one, and (3) possible loss of axial capacity if the upper column segment does not establish contact with the lower one. These phenomena are not a part of frame element formulations conventionally used in NLRHA. Consequently, efforts to represent the fracture of splices have relied on simplifications, e.g., a study by Stillmaker et al.[23] – which is currently the only NLRHA study with splice fracture, used a fiber-element based approach in which flexural failure did not trigger the loss of shear strength. While such studies provide some behavioral insights, they cannot be used to support definitive performance assessments owing to the lack of rigor in simulating the physics of splice response. Motivated by this, the main objectives of this study are:

1. To formulate a frame element that can represent the phenomenology of welded column splice fracture and post-fracture response in a physics-based manner. A novel material model and nonlocal mechanics-based approach are used to couple axial/flexural and shear response, and a kinematic formulation is used to represent the transfer of compressive stresses on contact. The general approach and element may be extended to other types of fracture in steel members.
2. To fully implement this formulation, with its attendant algorithmic and numerical aspects in an open-source structural simulation platform (i.e., Opensees[24]).
3. To conduct frame simulations demonstrating the formulation while also developing preliminary insights regarding frame response after splice fracture.

Given that most new buildings include improvements in connection design and materials specification for both column splices and beam-column connections, the primary application of this formulation will be for the evaluation of existing, pre-Northridge buildings that have deficient, un-retrofitted splices. Some aspects of the formulation (e.g., the ability to represent shear-loss) may have more general applicability other components that exhibit similar behavior.

The next section presents relevant background and prior work. This is followed by a discussion of the element formulation itself, and its numerical implementation. The paper concludes with a demonstrative exercise on a simple portal frame under dynamic pushover and a 20-story frame under seismic excitation.

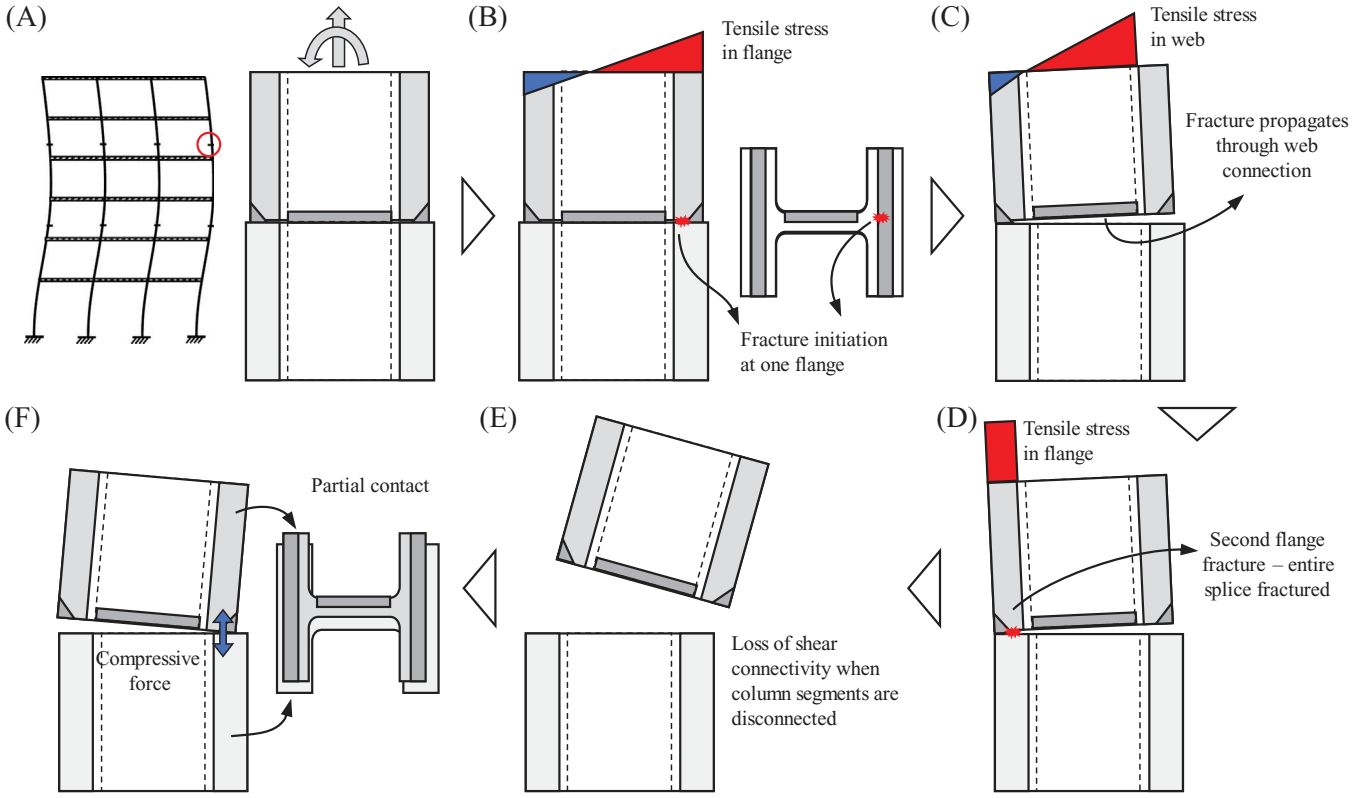

FIGURE 2 Phenomenology of fracture in welded splice: (A) Tensile stress in splice flange (B) Fracture initiation (C) Fracture propagation through web (D) Second flange fracture (E) Column segments disconnected (F) Contact of the upper column segment with the lower one.

2 | BACKGROUND

This section presents background including previous approaches to predicting splice fracture, the phenomenology of post-fracture response, and relevant element formulations and methodologies that may be leveraged to represent this in frame elements appropriate for NLRHA simulations.

2.1 | Phenomenology of post-fracture response of column splices

Figure 2 illustrates the phenomenology of fracture in welded column splices. Referring to Figure 2B, fracture typically initiates in the flange of the splice under a combination of axial force and moment, which results in tensile stresses in the flange. Experimental and analytical research by Shaw et al.,[6] Stillmaker et al.,[13] and Jhunjhunwala and Kanvinde[20] has resulted in approaches to estimate flange and web stresses at which the PJP splices fracture. This research has subsequently been implemented in analysis guidance documents,[21] as well as in software tools.[20] This work collectively provides a starting point for predicting stresses at which fracture will initiate. However, flange fracture is only the first event in a series of events that contribute to splice response.

Referring to Figure 2C and 2D (which show the progression of fracture through the splice), the fracture of one flange is followed by web fracture and eventually fracture of the second flange. Experiments suggest[22] that the web, which typically has similar PJP penetration to the flanges,[9,18] fractures almost immediately after the first flange. This may be attributed to the relatively high speed of crack propagation relative to the global loading rate, such that fracture is effectively "load-controlled." When the web splice is bolted (as is sometimes the case), the fracture propagation is more complex, and controlled by bolt hole patterns and the possibility of crack arrest at these holes (see experiments by Shaw et al.[6]). Each of these events occurs under high strain rates, owing to the load-controlled nature of the problem described above, and the sudden release of the strain energy associated with fracture. Once fracture propagates through the web and the second flange, the shear continuity of the column is destroyed, resulting in (a) changes to the natural frequency of the system

and (b) changes to the deflected shape and moment distribution in the adjoining column segments. The high strain rate associated with rapid unloading at complete fracture transmits high-amplitude stress waves with the potential to trigger failure elsewhere in the structure.[25]

The response at the splice level after complete fracture is controlled by interactions with global dynamic response. If it separates from the lower column, the disconnected column segment above the fractured splice moves freely as an upside-down cantilever without transferring axial, flexure, or shear force to the column segment below the splice, as shown in Figure 2E. In this case, the vertical load on the column is redistributed to other columns through the floor diaphragm and beams. The two column segments establish contact when the vertical uplift is less than the vertical displacement due to the bending of the floor diaphragm. This contact or reseating may be full or partial, as shown in Figure 2F, and is usually associated with dynamic impact resulting from instantaneous relative velocities of the two column segments. In this context, it is interesting to note observations after the Kobe earthquake that the fractured splices supported the dead loads even after partial reseating with a relative horizontal displacement in the range of 50 mm to 280 mm (2 in. to 11 in.) between the two column segments[17]; the columns themselves were 300 mm to 450 mm (12 in. to 18 in.) deep box sections. Shear transfer after reseating is primarily through friction and depends on the degree of axial compression transferred through bearing stresses at the reseated surfaces. When the column experiences uplift forces during subsequent loading, the upper column segment lifts off and loses contact with the lower one, re-initiating the process of unseating and reseating through the remainder of the shaking.

Following the discussion above, representing the phenomena of contact, separation, shear-loss, and reseating is critical for accurate simulation of the post-fracture response of splices. However, they are generally not incorporated in beam-column element formulations commonly used in NLRHA simulations and are challenging or computationally expensive to apply even in sophisticated continuum finite element simulations. This is problematic in the context of seismic performance assessment, where disregarding post-fracture response may not represent the physics of structural response (including force redistribution) and ultimately be inaccurate or highly conservative. Consequently, approaches have been proposed to represent such response providing a basis for developing the formulation presented herein. These are now briefly summarized.

2.2 | Fiber-elements with effective constitutive response

Researchers have proposed fiber-based beam-column elements[26] with constitutive response (i.e., uniaxial material models) that model loss of stress capacity to represent fracture and post-fracture response of structural members. These material models use a fracture criterion (e.g., a critical stress or strain), which triggers a change in constitutive response. Notable in this regard is the work by Hsiao et al.,[27] who employ a maximum strain-based criterion to determine the onset of fracture in braces of braced frames. In this approach, a uniaxial steel material model, *Steel02*, is modified to diminish its strength and modulus when the critical fracture criterion (defined as strain-range fracture model) is attained. More recently, Stillmaker et al.[23] proposed a new material model for simulating fracture in column splices. The column splice is modeled as a fiber element with a constant critical stress fracture criterion. The material model (discussed further in a subsequent section) is able to simulate the onset of fracture and post-fracture zero-tension capacity and bearing stresses in compression. Galvis et al.,[28] developed a material model for fiber-based simulation of beam-column connection. The model uses a stress-based fracture index instead of a constant critical fracture stress to determine the onset of fracture. This is particularly important for beam-column connections wherein fracture results from accumulated damage due to multiple loading cycles. The post-fracture gapping of the flange during separation and closure in compression is captured by the material constitutive relationship. In each of these models, the underlying element formulation (which uses cubic or Hermite shape functions) is unable to accommodate the loss of shear connectivity associated with the complete fracture of the section. As a result, even when the entire section fractures, it functions as an internal hinge with no flexural capacity but with the ability to transfer shear. This is unphysical and cannot reflect the redistribution of story shears to other columns.

2.3 | Rotational hinge or spring elements

Concentrated plasticity elements (usually in the form of rotational springs) are the prevalent approach to model steel connections[21] in NLRHA. A rotational spring in series with the elastic beam-column section simulates the connection

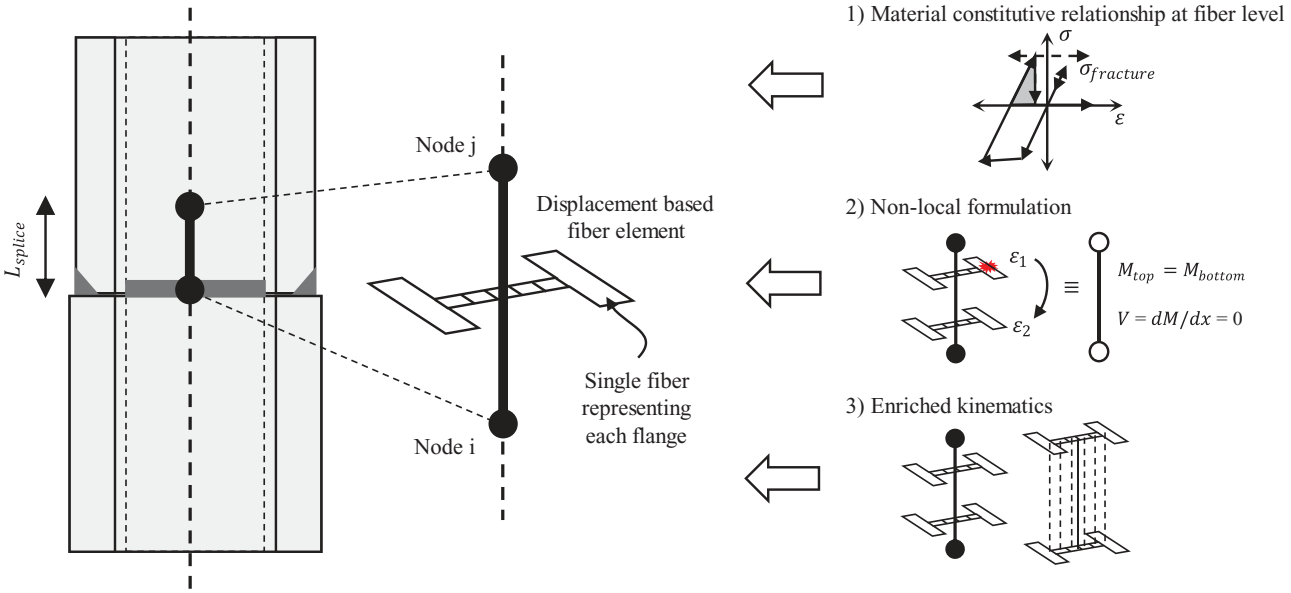

FIGURE 3 Splice element construct showing the displacement-based fiber element and enrichments.

flexural behavior, including – cyclic strength and stiffness degradation, post-peak softening, and residual strength.[29] These models phenomenologically simulate fracture by prescribing a steep negative slope (or "cap") in the moment-rotation response when a critical section strength or deformation (i.e., rotation) is reached. While expedient, these models cannot represent either axial-flexure interactions or the loss of shear strength and consequently, are best suited for connections (such as beam-column joints) where flexural response dominates. Concentrated hinge elements have also been used to model the shear and axial strength degradation of columns.[30] Uncoupled shear and axial springs are modeled in series with the beam-column element, and failure surfaces or limit curves are used to define the onset of failure in the respective modes. This approach may be used to represent the post-fracture shear loss functionally; however, it cannot simulate uplift and contact.

Other notable approaches for representing post-failure or fracture response include the Multiple Vertical Line Element Model (MVLEM), wherein fibers of the element are modeled as individual truss elements, all connected by a rigid link at each end.[31,32] The shear response of the element is simulated by a horizontal spring placed between the two nodes of the element, the behavior of which may or may not be coupled with the axial/ flexure response. The model has been implemented in OpenSees[24] exclusively for concrete shear walls with 2-dimensional RC panel behavior described by the Fixed-Strut-Angle-Model. Finally, element removal is used for progressive collapse assessment and alternate-force-path or redundancy assessment[33] and is suitable for instances when the damage in the element leads to complete loss of the element, such as crushing of reinforced concrete columns. Each approach provides a degree of promise in simulating aspects of post-fracture response in the context of splices. However, none effectively and efficiently represents the phenomenology of the post-fracture response of splices outlined above, which motivates the element construct described in the next section.

3 | ELEMENT CONSTRUCT

A new element, to effectively represent the various phenomena associated with column splices in a frame element-based framework, is formulated and implemented in the OpenSees[24] platform. The element, a two-node line element located at the splice location as shown in Figure 3, is derived by enhancing the fiber-based displacement beam-column elements with the following features:

1. A material constitutive model to simulate onset of fracture at the fiber level within the element.
2. A non-local formulation to simulate post-fracture loss of shear connectivity or "shear loss" at the element level.
3. Enriched kinematics of the element to represent the transfer of compressive stresses when the upper column segment establishes contact with the lower one.

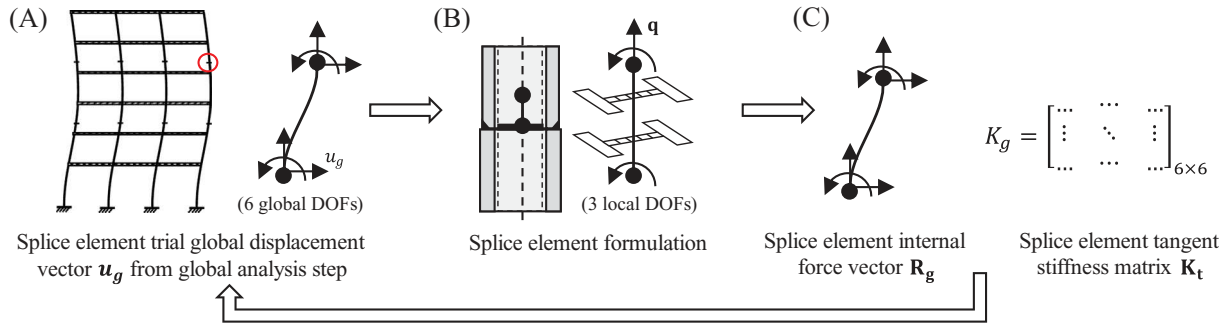

FIGURE 4 (A) Input to splice element from global analysis step (B) Splice element (C) Output to global analysis from splice element.

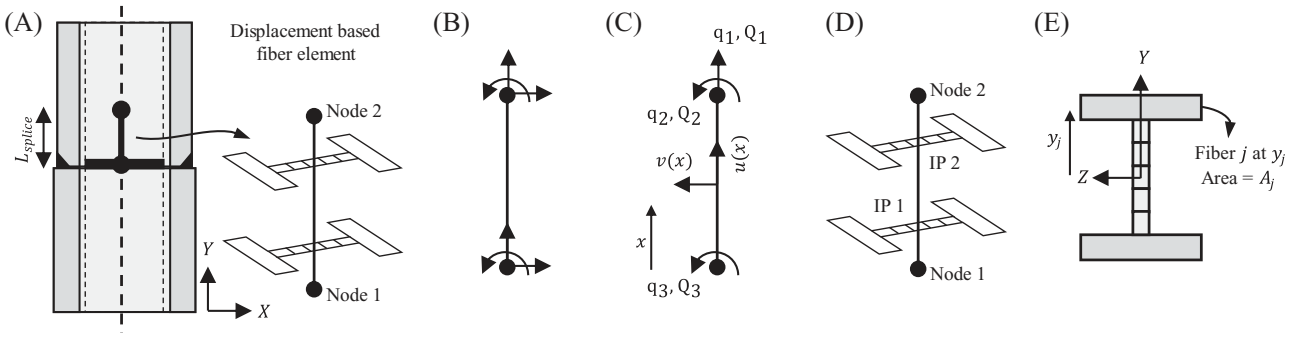

FIGURE 5 (A) Displacement-based fiber element (B) Global DOFs of splice element (C) Local deformation DOFs of splice element (D) Gauss Integration Points of splice element (E) Fiber discretization of splice element section.

The proposed approach relies on the general construct of the fiber-based displacement beam-column element.[26,34] As a result, this formulation retains aspects of conventional fiber elements that simulate elastic and inelastic axial-flexure interaction at the cross-sectional level, and the spread of plasticity through the element. These are important behaviors to represent in beam-columns besides the splice fracture itself. As such, the fiber element provides a suitable starting point for formulation to simulate the specific phenomenological responses of the splice fracture. The general construct of the fiber element is first described, followed by a detailed description of the enrichments and the additional considerations to facilitate the numerical convergence of a model with the splice element.

3.1 | General construct

The splice element is a two node, two-dimensional, displacement-based fiber element,[26,34] based on the Euler-Bernoulli beam theory, as shown in Figures 4B and 5A. The cross-section of the upper column is assigned to the element. The modeled length or the undeformed length of the element is denoted by L_{splice}. The element has six global degrees of freedom (DOFs) contained in the displacement vector, $\boldsymbol{u_g}$ as shown in Figure 4A. In the context of a standard predictor-corrector algorithm for non-linear analysis, a trial displacement vector is estimated based on applied loads and the tangent stiffness of the system. Subsequently, a solution is obtained by minimizing an appropriate residual based upon internal forces, necessitating force recovery or state determination for all elements.[35] The global end displacements (and the displacement increment during an analysis) are passed to the splice element to determine the element state, i.e., the internal force vector $\boldsymbol{R_g}$ and the 6×6 element global tangent stiffness matrix, $\mathbf{K_t}$ as shown in Figure 4C. On eliminating the rigid body modes provided by the shear continuity, the global DOFs of the element are transformed to the local coordinate system with deformation degrees of freedom, as shown in Figure 5B and 5C. The element end displacement vector $\mathbf{q}$ in local DOFs may then be expressed as:

$$\mathbf{q} = \begin{bmatrix} q_1 & q_2 & q_3 \end{bmatrix}^T \tag{1}$$

and the corresponding end forces vector Q as:

$$\mathbf{Q} = \begin{bmatrix} \mathrm{Q}_1 & \mathrm{Q}_2 & \mathrm{Q}_3 \end{bmatrix}^T \tag{2}$$

where q_1 and Q_1 are the end axial displacement and end axial force respectively, q_2 and q_3 are the end rotations, and Q_2 and Q_3 are the end moments. Due to the absence of shear deformations in the Euler-Bernoulli beam formulation, the shear force is eliminated from the element end force vector during the transformation. The transformation to local coordinates may be performed with respect to the initial configuration of the element, referred to as a linear transformation, or with respect to the current configuration in the analysis, referred to as a corotational transformation. The former is adequate for small deformation problems, while the latter is suitable for situations involving large deformations. Before splice fracture, element deformations are small, and a linear transformation may be used. After the fracture of the entire splice section, when the splice element simulates the uplift of the upper column segment, the transformation is not important because the splice element does not have a force. However, when the splice element is in compression after fracture, the additional kinematics for simulating contact influences the type of transformation used; this is discussed later.

The axial and transverse displacements at each section along the element, denoted by $\mathbf{u}(x)$, may be expressed as:

$$\mathbf{u}(x) = \begin{bmatrix} u(x) \\ v(x) \end{bmatrix} = \mathbf{N}(x)\,\mathbf{q} \tag{3}$$

where $u(x)$ is the axial displacement and $v(x)$ is the transverse displacement, at location x along the element. $\mathbf{N}(x)$ is a matrix of the displacement shape functions using cubic Hermite polynomials for transverse displacement field and linear Lagrange polynomial for the axial displacement, expressed as:

$$\mathbf{N}(x) = \begin{bmatrix} \xi & 0 & 0 \\ 0 & \xi^3 - 2\xi^2 + \xi & \xi^3 - \xi^2 \end{bmatrix} \tag{4}$$

where $\xi = x/L$ and L is the element length. The interpolated axial and transverse displacement of the element may be transformed to the section deformation vector, $\mathbf{d}$, based on the assumption of Plane Sections Remain Plane (PSRP), such that:

$$\mathbf{d}(x) = \begin{bmatrix} \varepsilon(x) \\ \phi(x) \end{bmatrix} = \begin{bmatrix} u'(x) \\ v''(x) \end{bmatrix} = \mathbf{B}(x)\,\mathbf{q} \tag{5}$$

where $\varepsilon(x) = u'(x)$ is the section axial strain; $\phi(x) = v''(x)$ is the section curvature at a given location x along the element; and $\mathbf{B}(x)$ is the matrix relating section deformation to element end displacements, consisting of shape function derivatives at that location. The section force vector $\mathbf{D}(x)$ that consists of section axial force, $P(x)$ and bending moment, $M(x)$, may be expressed as:

$$\mathbf{D}(x) = \begin{bmatrix} P(x) \\ M(x) \end{bmatrix} = \mathbf{C}(x)\,\mathbf{d}(x) \tag{6}$$

where $\mathbf{C}(x)$ is the section stiffness matrix relating the section force vector to section deformation vector. The Principle of Virtual Displacement (PVD) is now applied to determine the element end forces in local DOFs as:

$$\mathbf{Q} = \int_0^L [\mathbf{B}(x)]^T \mathbf{D}(x)\,dx = \sum_{i=1}^{N_p} \Omega_i [\mathbf{B}(x_i)]^T \mathbf{D}(x_i) \tag{7}$$

The integral in the above equation is evaluated using numerical quadrature over N_p number of sections or Integration Points (IPs) along the element. For the displacement-based element with displacement shape functions given by Equation (4), two IPs allow for accurate estimation of the integral using Gauss-Legendre integration rule. The formulation of the splice element presented henceforth considers the number of IPs to be fixed as two, i.e., $i = 1$ and 2 as shown in Figure 5D. The term Ω_i in the expression denotes the quadrature weight associated with each IP, which are equal for both

the IPs when two IPs are used. Similar to the element end forces, the element tangent stiffness matrix in local DOFs may also be recovered using PVD:

$$\mathbf{K}_{\mathbf{t}}' = \int_0^L [\mathbf{B}(x)]^T \mathbf{C}(x)\,\mathbf{B}(x)\,dx = \sum_{i=1}^{N_p} \Omega_i [\mathbf{B}(x_i)]^T \mathbf{C}(x_i)\,\mathbf{B}(x_i) \tag{8}$$

The element internal force vector, $\boldsymbol{R_g}$ and the tangent stiffness matrix, $\mathbf{K_t}$ are now obtained using the geometric transformation from local to global coordinates. In the case of linear transformation, which is used for the splice element, the magnitude of the end moments is same in both global and local coordinates because the initial configuration is used as a reference. The shear force, which is constant over the element length, is calculated from the element end moments as:

$$V = \frac{Q_2 + Q_3}{L_{splice}} \tag{9}$$

In the fiber element formulation, the section of the element is discretized into multiple fibers as shown in Figure 5D. This allows the sectional response at each IP to be dictated by material response of individual fibers, thus capturing the axial-flexure interaction at the sectional level. Using the fiber discretization, the section force vector and the section stiffness matrix at an IP, shown in Equation (6), are now expressed in Equations (10) and (11) respectively:

$$\mathbf{D}(x_i) = \begin{bmatrix} P(x_i) \\ M(x_i) \end{bmatrix} = \begin{bmatrix} \sum_{j=1}^{N_f} \sigma_{j(i)} A_j \\ \sum_{j=1}^{N_f} \sigma_{j(i)} A_j y_j \end{bmatrix} \tag{10}$$

$$\mathbf{C}(x_i) = \begin{bmatrix} \sum_{j=1}^{N_f} E_{j(i)} A_j & -\sum_{j=1}^{N_f} E_{j(i)} A_j y_j \\ -\sum_{j=1}^{N_f} E_{j(i)} A_j y_j & \sum_{j=1}^{N_f} E_{j(i)} A_j y_j^2 \end{bmatrix} \tag{11}$$

where $\sigma_{j(i)}$ is the uniaxial stress at the jth fiber at the ith IP; $E_{j(i)}$ is the material tangent stiffness at the jth fiber at the ith IP; A_j is the area of the jth fiber; y_j is the location of the centroid of jth fiber; x_i is the location of the ith IP; and N_f is the number of fiber discretization in the section at ith IP. The sections at the two IPs may, in general, have different fiber discretization; however, the formulation for the splice element uses the same discretization at both sections as shown in Figure 5E. The uniaxial strain at a fiber location is obtained from the sectional axial strain and the section curvature as:

$$\varepsilon_{j(i)} = \varepsilon(x_i) - y_j \phi(x_i) \tag{12}$$

The uniaxial stress and material tangent stiffness at a fiber, used in Equations (10) and (11), is evaluated from the uniaxial strain, $\varepsilon_{j(i)}$ at the fiber location and the material constitutive relationship, expressed as:

$$\sigma_{j(i)}, E_{j(i)} = f\left(\epsilon_{j(i)}\right) \tag{13}$$

where $f()$ is the constitutive relationship. The formulation described above captures the pre-fracture behavior of the splice element, through the well-established displacement-based fiber element formulation. This forms the basis for proposed enhancements aimed at developing a new splice element capable of capturing the onset of fracture and the post-fracture response. Next, the adopted material model, which governs the pre-fracture behavior and captures the onset of fracture at the fiber level, will be discussed.

3.2 | Simulating fracture at fiber level

Once the overall element formulation is established, an appropriate constitutive model is required to reflect the fracture response at the fiber level. In this regard, the initiation of fracture in column splices may be considered to be controlled by the flange or web stress depending on flange/web thickness and weld penetration. A uniaxial constitutive model developed by Stillmaker et al.[23] is used in the proposed approach. This model can reflect the onset of fracture and the subsequent post-fracture response at the fiber material level. This material model is constructed by arranging a steel bilinear material

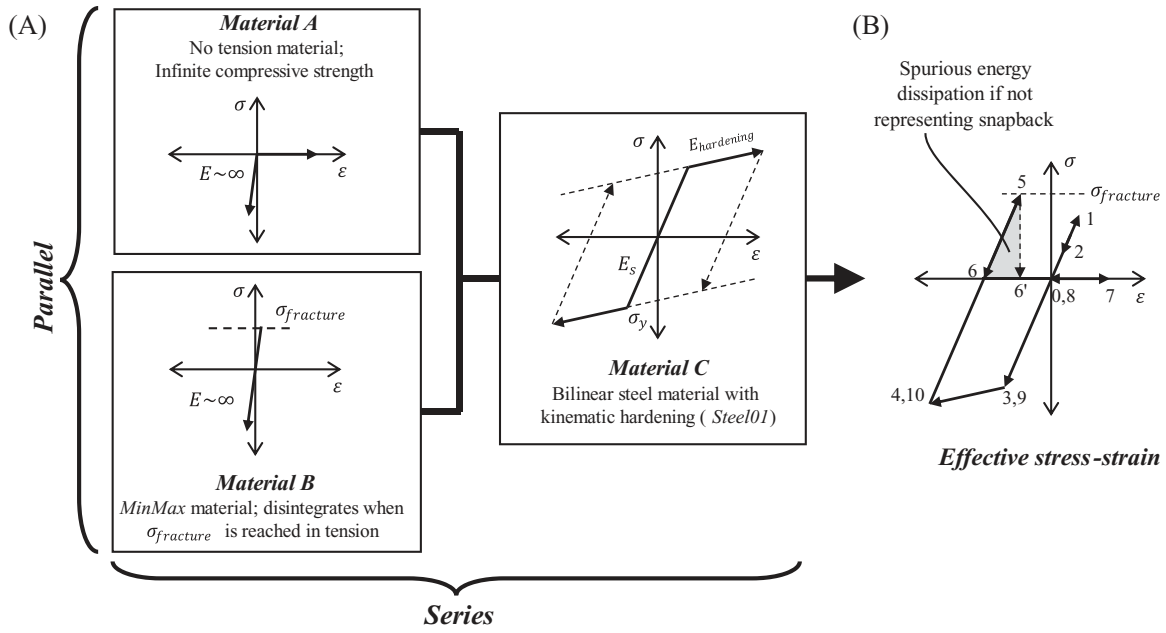

FIGURE 6 Material model for simulating fracture at fiber level.

(*Steel01* in OpenSees) in series with a parallel combination of a no-tension material and a *MinMax* material, as illustrated in Figure 6A. The *MinMax* material, which disintegrates when a maximum or minimum stress is reached, is only assigned a maximum tensile stress equal to the critical fracture stress of the corresponding fiber, $\sigma_{fracture}$. Figure 6B shows the resulting cyclic response, where numerically marked points illustrate the sequential evolution of stress-strain history. The key features and implications of the material model are described below:

1. The material is elastic in tension until a fracture stress, $\sigma_{fracture}$ is reached in a fiber at an IP. Referring to Figure 6B, path 0–1 indicates initial elastic loading, path 2-3-4 indicates unloading and compressive yielding, and point 5 shows fracture upon reloading in tension at $\sigma_{fracture}$. This critical fracture stress of the flanges and webs of the splices can be determined using approaches provided by Stillmaker et al.,[13] ATC 114,[21] and Jhunjhunwala and Kanvinde[20] - this is typically on the order of 100–200 MPa (i.e., 25–50% of the yield stress of the material), indicating that fracture is predicted to occur when the section is still elastic. The recent approach by Jhunjhunwala and Kanvinde[20] allows determining the fracture stress in different loading scenarios. The material model can be modified to include changing fracture stress at each analysis step based on the axial-flexure loading scenario. However, to emphasize on the element formulation, a constant fracture stress independent of the loading type is used in this study. It should be noted that fracture stress is defined as the far-field stress (specifically the stress in the flange fiber) in the upper column section, which, when reached, severs the entire flange at once. Thus, the splice element is modeled using the upper column cross-section with each flange modeled as a single fiber.
2. Once the critical fracture stress is reached in a fiber at an IP, the material loses all stress capacity in tension as the *MinMax* material disintegrates. The remaining "no-tension" material in series with the *Steel01* material is able to simulate 'snap-back' wherein the strain returns elastically to zero before increasing back up to the applied strain,[23] as indicated by path 5-6-7 in Figure 6B. This is different from simulating fracture through a negative slope, as indicated by path 5–6'-7, which leads to spurious energy dissipation (see shaded region in Figure 6) and is inconsistent with brittle fracture.
3. After fracture, the material loses all strength in tension. The strength in compression is maintained as indicated by path 7-8-9-10. Since the stress in compression does not typically increase beyond the expected yield strength of steel before fracture, the *Steel01* material model may be replaced with a simple elastic material for convenience.

The material model described above effectively reflects the onset of fracture and the loss of tensile strength after fracture at the fiber level. It should be noted that each fiber within the element has two IPs (along the length), with the potential for material fracture at one of the IPs and elastic unloading without fracture at the other IP, because the strains at two

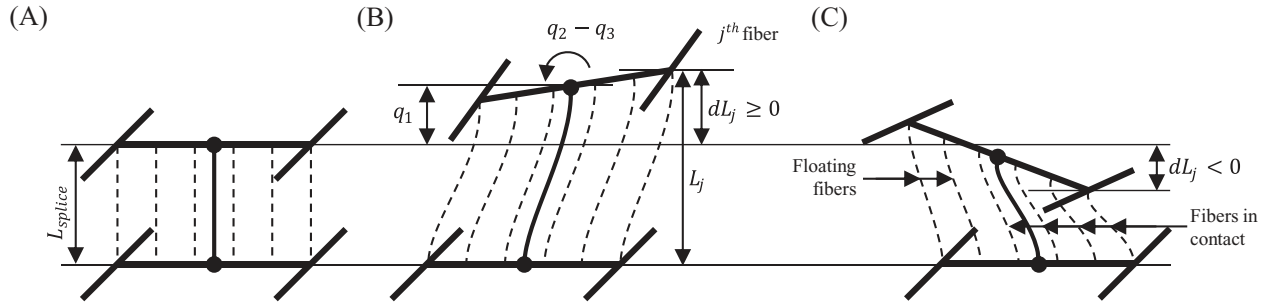

FIGURE 7 Kinematics after fracture: (A) Undeformed configuration (B) Floating (C) Partial contact after fracture.

longitudinal locations along a fiber may be different. The difference is primarily due to the flexural component of the deformation interpolation, which is cubic and represents a linear curvature distribution over the length. The implication of this difference in strains (and consequently stresses) along the length is a moment gradient, which results in an effective shear force in the element section. This is contrary to the expected response (i.e., no shear when all fibers have fractured in tension) and is an artifact of the underlying deformation interpolation, which cannot accommodate the discontinuous post-fracture displacements. The non-local implementation discussed next ensures that the fiber fractures at both IPs simultaneously and that the post-fracture shear loss in the splice element is simulated.

3.3 | Simulating the loss of shear strength after the splice has fractured

When the material at an IP of a fiber fractures, the subsequent response of the fiber may follow one of two modes, each with distinct physical phenomena. These modes are: (a) the upper column segment disconnects from the lower one at the fiber location, or (b) the upper column segment establishes contact with the lower one. In mathematical terms, the first scenario occurs when the relative vertical end displacement of a fiber, dL_j, is greater than zero, as shown in Figure 7B. Essentially, the vertical distance between the two ends of the deformed fiber, L_j, is greater than the undeformed length of the fiber, as shown in Figure 7A, which is the same as the undeformed length of the splice element, L_{splice}. This is referred to as "floating" henceforth. The contact scenario relates to Figure 7C, where the relative vertical end displacement of the fiber is less than zero. Some fibers of the splice element may be floating, and some may be in contact depending on the element end displacements. The relative vertical end displacement of a fiber is determined from the element end displacement as:

$$dL_j = \mathrm{q}_1 - y_j\,(\mathrm{q}_2 - \mathrm{q}_3) \tag{14}$$

where q_1 represents the axial deformation in local DOFs of the splice element, which is also the relative vertical displacement of the two nodes of the splice element in global DOFs because a linear geometric transformation is used for the element. It is essential to note that dL_j does not represent the change in length of the fiber itself, which also undergoes a lateral deformation and additional deformation due to arcing.

In the case of floating, i.e., $dL_j \geq 0$, a fiber should physically behave as non-existent. Numerically, this means that the contribution of the fiber to the section stiffness and section forces at both the IPs, given by Equation (10) and (11), respectively, should be zero. However, the displacement-based element with the material model cannot ensure this for all floating scenarios after fracture: (a) when the material at one IP fractures and the material at the other IP unloads elastically without fracture, and (b) the displacement field in the splice element is in double curvature, i.e., it contains flexural contributions. In the former, tensile strain during uplift generates tensile stress at the elastically unloaded IP. In the latter, compressive strain may be computed at an IP of the fiber even when the upper column segment is floating, as estimated from Equations (5) and (12); this leads to compressive stress at the IP of the fiber. Both scenarios result in a non-zero contribution of the fiber to the section stiffness and the section forces at one of the IPs. When the entire upper column segment disconnects from the lower one, i.e., all the fibers of the splice element are fractured, these scenarios lead to a moment gradient along the element and transfer of shear through the element, i.e., $\mathrm{Q}_2 \neq -\mathrm{Q}_3$, in Equation (9).

An approach inspired by non-local formulations[36,37] is developed to represent the shear loss subsequent to fracture of the entire section. More specifically, at and after the instant an IP of a fiber fractures, the constitutive response at each IP

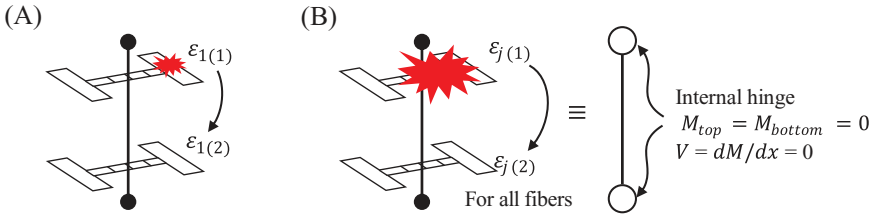

FIGURE 8 (A) Non-local transfer of strains (B) Equivalent element with internal hinges on both ends after entire section fracture.

in the fiber is governed by the *maximum* of the strains at the IPs when the fiber is floating, rather than the local strain at the IP itself – similar to a non-local formulation. This may be expressed as a modification to Equation (13), i.e.,

$$\sigma_{j(i)}, E_{j(i)} = f\left(\max\left(\epsilon_{j(1)}, \epsilon_{j(2)}\right)\right) \text{ given } dL_j \geq 0 \tag{15}$$

The proposed approach results in the following: (1) the same strain is used at both IPs at the instant any IP fractures, ensuring simultaneous fracture at both IPs, and (2) the maximum tensile strain, including the effect of curvature, is positive during floating, preventing any spurious compressive stresses at the IPs; this results in the computation of zero section forces and section stiffness matrix at both IPs, regardless of the curvature of the element. The latter ensures that the element forces through the splice, including shear, are zero in all scenarios when the entire upper column segment is disconnected from the lower one. The implementation is analogous to two flexure hinges at the end of the splice element when floating, as shown in Figure 8. The approach above simulates the physical response of the fibers when floating in a displacement-based element framework. The modifications to element kinematics to represent the transfer of compressive stresses when the upper column segment establishes contact with the lower one are discussed in the next section.

3.4 | Enriched kinematics to represent transfer of compressive stresses on contact

The motion of the fractured segments of the column poses some additional challenges, primarily because the splice element (which is effectively a Euler-Bernoulli beam) cannot represent the discontinuous deformation field that arises during this phase of response. Various phenomena may be active during this phase, including: (1) full or partial seating of the upper column segment on the lower one, resulting in the compressive stresses due to bearing on contact, and consequently axial compression and moment, and (2) the associated mobilization of friction, resulting in re-establishment of shear connectivity between the two segments. An issue arises as a consequence of the non-local formulation introduced above with the objective of representing shear loss. Figure 7C illustrates this issue. Specifically, the fractured surface of the upper column segment may establish contact with the lower column segment (see right-hand side flange), with a transfer of compressive bearing. However, due to the cubic deformation (and linear curvature) interpolation, a positive (i.e., tensile) strain may still be computed at one of the IPs along the fiber at this location; this is the converse of the situation described in the previous section wherein a compressive stress is computed an IP even after fracture, due to linear curvature interpolation. In conjunction with the non-local formulation, this results in the loss of axial stress capacity as well, because Equation 15 implies that the larger strain of the two IPs (i.e., 0 in this case) is used for computation of stress. This is clearly unphysical since it fails to capture compressive stresses on contact.

To circumvent this problem, the following protocol is adopted. It is assumed that the upper column segment at a fiber location establishes contact with the lower one when the relative vertical distance between the two ends of the corresponding fiber, dL_j calculated from Equation (14), is less than the undeformed length of the fiber, i.e., L_{splice}. Consequently, the fiber may be considered to be in contact with the lower segment when:

$$dL_j < 0 \tag{16}$$

The above criterion disregards the horizontal displacement between the two ends of the fiber, which results in imperfect seating of the upper column segment on the lower column segment. This assumption is considered adequate within the context of this study to represent contact when the horizontal displacement of the upper column segment relative is not high enough for the column to unseat. When the criterion is satisfied, a compressive strain of dL_j/L_{splice} is specified at both the IPs of the fiber in contact. The same strain at both IPs enforces a uniform displacement field in the fiber, allowing

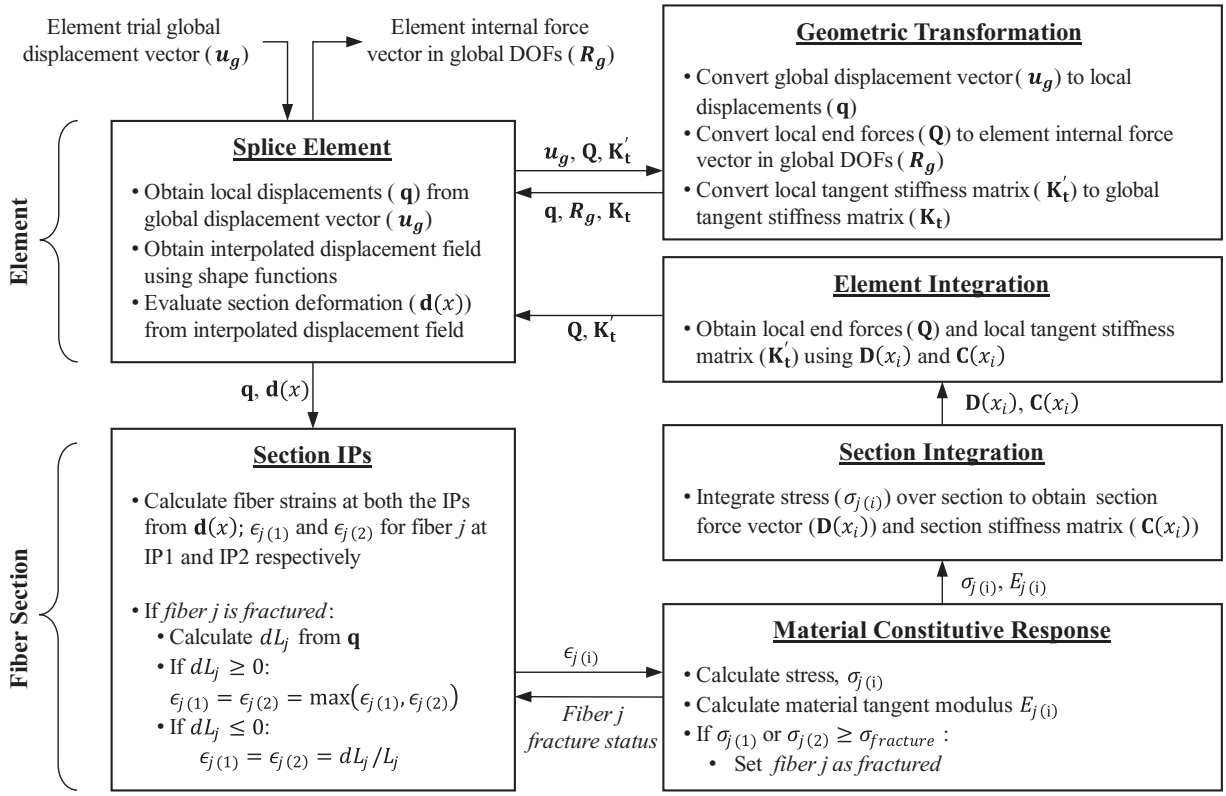

FIGURE 9 Flow diagram for force recovery process of the splice element.

the computation of compressive stresses at both IPs without generating a moment gradient. Essentially, the fiber behaves as a linear truss element when the criterion for contact is satisfied. Thus, Equation (13) to determine the stress and material tangent stiffness at the IPs is modified to:

$$\sigma_{j(i)}, E_{j(i)} = f\left(\varepsilon = \frac{dL_j}{L_{splice}}\right) \text{ given } dL_j < 0 \tag{17}$$

The above approach ensures that the fiber in contact transfers compressive forces regardless of the curvature of the element, i.e., the strain assignment supersedes the strain calculation from the interpolated displacement field which may be tensile at one of the IPs. In this manner, the portion of the section in contact is still able to transmit moment (due to the stress gradient) but cannot transmit shear. Moreover, the moment transmitted this way is dependent on the local deformation of the cross-section, rather than the interpolated curvatures. This is a purely expedient consideration, to achieve reasonably realistic response when the cubic shape functions are clearly insufficient to replicate the discontinuous deformations associated with partial contact.

As a consequence of the non-local modification (described in the previous section) and the section kinematics (described above), the section forces and section stiffness matrix at both the IPs are equal after all fibers are fractured in the splice element (resulting from equal strains at both the IPs in both the modifications). Therefore, the element end forces are equal and opposite, i.e., $Q_2 = -Q_3$, resulting in zero shear force through the element in all scenarios, whether partial or full contact. This is a limitation of the adopted methodology.

The splice element formulation described above is implemented within OpenSees as a new element, *dispBeamColumnSplice*, by modifying the existing *dispBeamColumn* element. It is referred to as the Splice Fracture Element (SFE) hereafter. A schematic representation of the computational implementation is shown in Figure 9. Beyond the element itself, modifications are required in the numerical model to adequately capture anticipated behavior at the global level and facilitate convergence beyond the initial fracture. These adjustments are discussed in the next section.

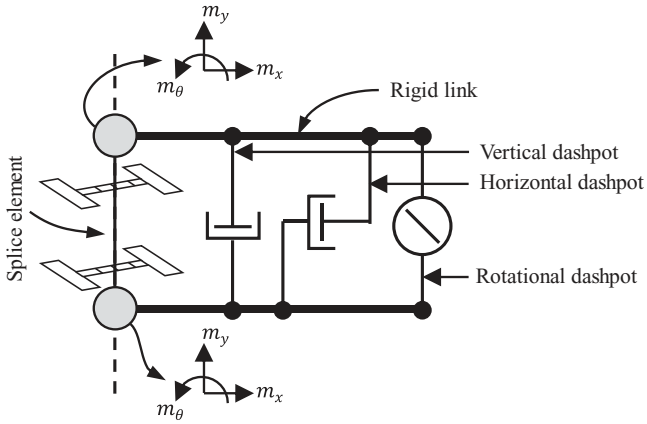

FIGURE 10 Additional considerations for splice element.

3.5 | Additional considerations to facilitate convergence

In addition to the element construct for simulating splice fracture and post-fracture response, some considerations are needed to simulate the expected behavior of the SFE and the convergence of global analysis. In this context, it is important to note that the SFE (as formulated and implemented above) results in "snapback" response that cannot be simulated in a general sense through conventional quasi-static simulations (since no static solution may exist[35]), albeit arc-length approaches may be used to obtain solutions of snapback in specific situations successfully. As a result, the SFE is suited for application within dynamic simulations (such as NLRHA), which are able to simulate snapback directly. Within this setting, a major obstacle to convergence arises from the abrupt release of a large amount of strain energy when a splice fractures. This may be addressed by assigning appropriate nodal masses, damping, and selection of analysis parameters for global convergence; this is now described.

Damping: Conventionally, initial stiffness and mass-proportional Rayleigh damping is assigned to the building model when performing non-linear time history analysis. However, assigning initial stiffness proportional damping to the SFE, given its high stiffness before fracture (due to its small length), results in unnaturally high damping at the splice location. The high damping is acceptable when the SFE has not fractured. When the SFE fractures, the combination of high damping and the relative velocity between the element nodes leads to an unphysical computation of force transfer from the upper to the lower column segment. This is critical, especially when the SFE is floating after fracture. On the other hand, assigning current stiffness proportional damping reduces the element damping to zero upon fracture. Since fracture is an energy release phenomenon, the absence of damping leads to convergence issues due to instantaneous unbounded velocities between the two splice nodes. Thus, an optimal approach is to assign very low initial stiffness proportional damping to the SFE, which regulates the unbounded velocities while minimizing force transfer through damping. Physically, this damping may be interpreted as viscous regularization to delay the sudden release of energy.[38] Alternatively, no Rayleigh damping may be assigned, and three dashpots, each with a viscosity lower than the damping in neighboring columns, may be added in parallel with the SFE (as shown in Figure 10). A higher value of viscosity results in faster numerical convergence but will allow larger damping forces after fracture. A lower viscosity value is susceptible to convergence issues, but it will minimize the damping forces. In this study, it is determined that a dashpot constant (i.e., viscosity) of the order of $1/100^{\text{th}}$ of the contribution of the upper or lower column segment to the damping matrix in the corresponding direction is sufficient to achieve convergence without increasing the damping force to the extent that it affects the numerical solution.

Nodal mass: In contrast to traditional NLRHA, wherein nodal masses are conventionally provided only at the structural joints, additional considerations are necessary when simulating frames using the SFE element, namely: (1) masses must be assigned at each node within the column (composed of multiple elements), because local inertial effects due to the mass of the column itself, i.e., between the structural joints are non-negligible given the high local accelerations immediately after fracture, and (2) masses must be assigned in both the horizontal and vertical directions, because these high instantaneous accelerations occur in both directions. These measures collectively ensure numerical stability and regularize the system dynamics without generating an unphysical response at the structural scale.

Analysis parameters: As mentioned previously, the snap-back phenomenon associated with splice fracture is best simulated in fully dynamic nonlinear simulations (such as NLRHA) with the features described above. Within this, standard

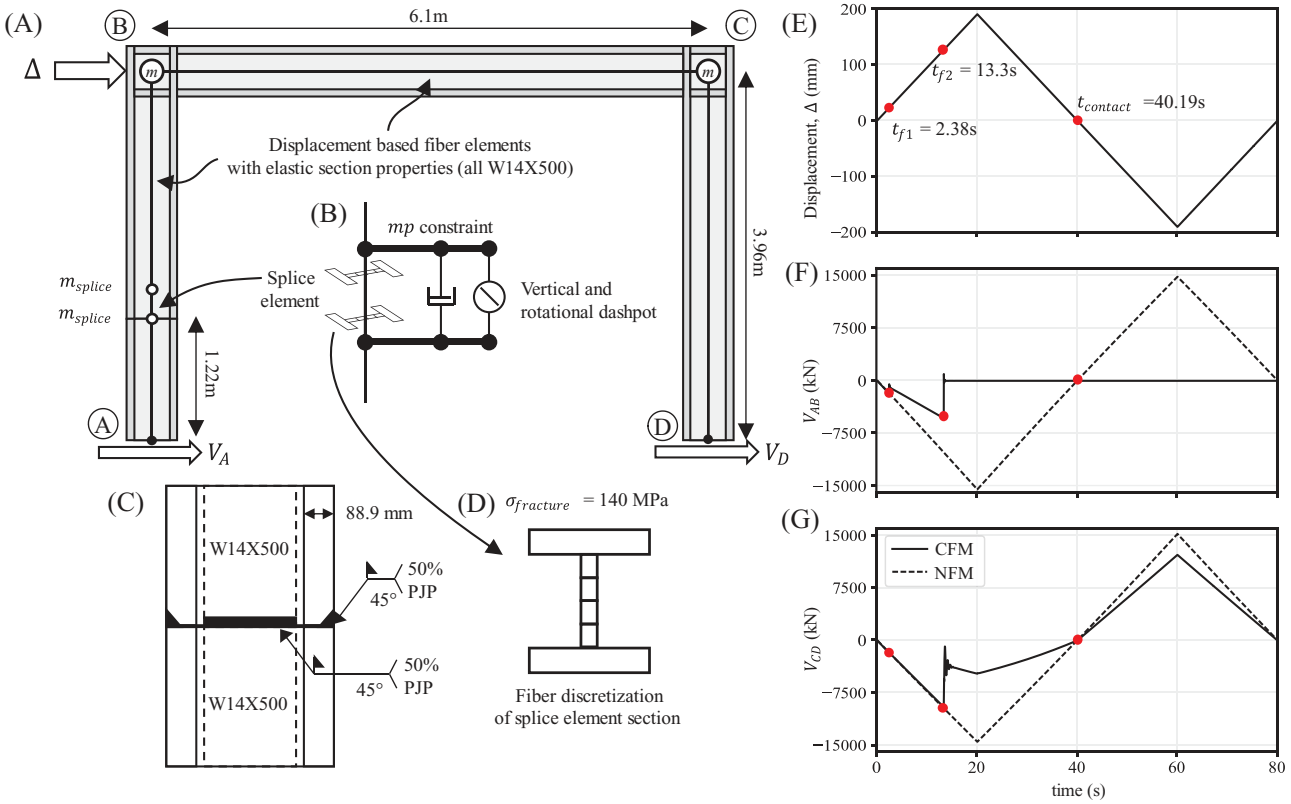

FIGURE 11 (A) Elastic portal frame with splice element, (B) Splice element with dashpots, (C) Splice connection details, (D) Fiber discretization of splice element section, (E) Applied displacement, (F) Base shear in column AB, (G) Base shear in column CD.

dynamic solution methods, like Newmark with Newton's algorithm,[35] were determined to be sufficient for achieving convergence in the analysis. However, to ensure convergence after multiple instances of fracture, it was also noted that the analysis time step needs to be refined, possibly to as low as 1e-5 sec (for the structures examined within this study). This small step is necessitated by the highly nonlinear behavior of reseating and uplifting at the splice location. In structures with multiple splices, the system may become unstable when all splices at a given floor level fracture. Beyond this critical point, the building detaches from the floor level where all splices are fractured. In such cases, explicit analysis, with a further reduction in the time step, is required to simulate the response. In this study, it is assumed that such a response is not within the scope of structural performance assessment and may be considered equivalent to the collapse or complete failure of the structure.

With the above considerations, the following section demonstrates and examines the performance of the SFE through two sets of simulations: (1) a dynamic cyclic pushover analysis of an elastic portal frame with fracturing splices and (2) NLRHA of a 20-story building subjected to a high-intensity ground motion.

4 | DEMONSTRATIVE APPLICATION TO ONE-STORY FRAME

The SFE element construct is applied to simulate a one-story, one-bay portal frame subjected to a set of reversed loading cycles applied as displacements to the top left-hand side node B, as shown in Figure 11A. This model exhibits all relevant aspects of response that are the focus of the SFE, i.e., fracture under tensile stresses, resulting in loss of flexural and, ultimately, shear capacity, followed by post-fracture floating and contact of the disconnected column segments. Moreover, the model is relatively simple, allowing for the detailed demonstration and evaluation of component-level response (including the response of individual fibers) and its interaction with the global structural response. This is particularly important because no experimental data exist on splices with documented post-fracture response. As shown in Figure 11A, all members are W14 × 500 (see dimensions in Figure 11C), and only one of the columns, column AB on the left-hand side, incorporates a welded column splice with 50% Partial Joint Penetration (PJP) in both flanges and the web.

Loading is applied as a displacement time history (Figure 11E) at the top story level at node B. The loading is applied in a dynamic sense because the localized snap-back associated with splice fracture does not theoretically permit a quasi-static solution.[35] The loading rate is selected to be sufficiently slow (i.e., 10 mm/s relative to the expected rate of structural harmonic response, expected to be on the order of 300 mm/s for a peak story displacement of 190 mm, which is applied in the loading) to avoid imposed dynamic effects. The maximum displacement is selected to induce splice fracture during displacement in the positive direction, as shown in Figure 11A. The absence of a splice in the right-hand side column, column CD, ensures overall structural stability after the complete fracture of the splice in column AB, encouraging convergence and providing an opportunity to evaluate the effectiveness of simulating fracture. The modeling aspects of the model developed in OpenSees are discussed below:

1. Column CD, beam BC, and column segments above and below the splice in column AB are modeled as displacement-based fiber elements with an elastic steel material (Elastic modulus, E = 200 GPa). A corotational transformation is assigned to these elements to appropriately simulate anticipated large displacements and rotations after the fracture of the splice. Rigid joint offsets are not modeled.
2. The splice is modeled using the developed SFE, *dispBeamColumnSplice*, with a length of 50 mm (2 in.). Two integration points are assigned within each splice element, and a linear transformation is applied to the splice element as required by the formulation. Each flange is modeled as a single fiber, as shown in Figure 11D, assuming that fracture severs the entire flange simultaneously. The material model proposed by Stillmaker et al.,[23] illustrated in Figure 6, is assigned to splice element fibers, with *Steel01* material replaced by an elastic material. The fracture stress, $\sigma_{fracture}$ for the *Min-Max* material is set to 140 MPa (which is $0.36F_y$), as obtained from the methodology developed by Jhunjhunwala and Kanvinde,[20] using the assumed flange and web penetrations, and a CVN value of 13.6 J at 21.1°C. Note that these are representative values used within the context of a demonstrative exercise.
3. Initial stiffness proportional Rayleigh damping is assigned to all the elements except the splice element. Vertical and rotational dashpots are provided in parallel with the splice element, as shown in Figure 11B, to regulate the dynamics of the model, mitigating the possibility of unbounded relative velocities across the splice element. The dashpot constant (i.e., viscosity) is selected to be 1/100th of the order of contribution of the upper column segment to the damping matrix; this is sufficient to achieve convergence without increasing the damping force to the extent that it affects the numerical solution.
4. A mass of 45,000 kgs (corresponding to a weight of 100 kips) each is assigned to the top two nodes, node B and node C; the value is selected to provide a realistic time period of 0.15 sec. No vertical force is applied to these nodes to simplify the model and exclude gravitational loads. Additionally, masses reflecting the half weight of the upper and lower column segments are attached to the top and bottom splice element nodes; these are taken to be 900 kgs (2 kips) at both nodes for convenience.

An additional simulation is conducted without the splice element (i.e., with continuous columns on both the left-hand and right-hand side) to provide a benchmark solution reflecting the condition wherein the splice remains intact. In subsequent discussion, this model is referred to as the *No Fracture Model* (NFM), while the model with the SFE is referred to as the *Complete Fracture Model* (CFM). As noted earlier, Figure 11E shows the applied loading, whereas Figure 11F show the evolution of the base shear in columns AB and CD, respectively. Figure 12 focuses on the SFE itself, providing a detailed view of the evolution of forces within it. Specifically, Figure 12B show the evolution of axial force, bending moment, and shear within the SFE. Figure 12E illustrate the splice kinematics and internal fiber stresses (as recovered from the SFE data) at three key instants during the loading history. These loading instants are significant in the following way: t_{f1} = 2.38s corresponds to the instant at which the left-hand side flange of the splice fractures, t_{f2} = 13.3s corresponds to the instant at which the right-hand side flange of the splice fractures resulting in severance of the entire section, and $t_{contact}$ = 40.19s corresponds to the instant when the right-hand side flange of the upper column segment establishes contact with the lower column segment. Referring to Figures 11 and 12, the following observations are made, corresponding to phases in the loading history:

1) Referring to Figures 11F and 11G, the response of the NFM model is unremarkable, except that local dynamics are not noticeable, confirming that the applied loading rate is sufficiently slow. The response of the CFM is identical to that of the NFM until the first flange fractures at t_{f1}; this is verified to occur at the fracture stress as specified in the SFE, as shown in Figure 12E.

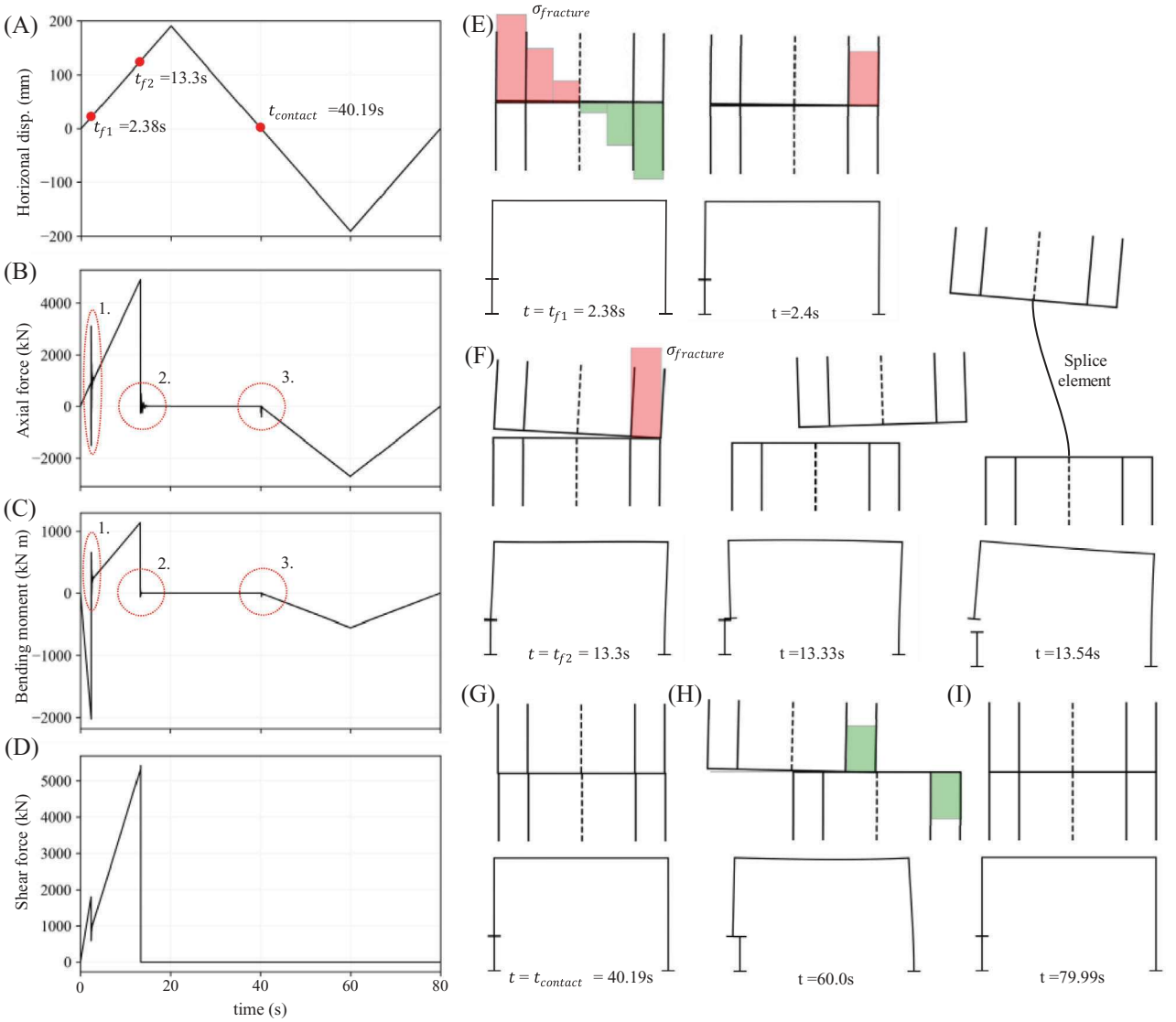

FIGURE 12 (A) Applied displacement, (B) Axial force through splice element, (C) Bending moment at bottom of splice element, (D) Shear force through splice element, (E) Left-hand side flange fracture accompanied by fracture of web, (F) Right-hand side flange fracture severing the entire splice, (G) Right-hand side flange in contact with lower column segment, (H) Right-hand side flange sliding on web while maintaining contact with lower column segment, (I) Right-hand side flange losing contact.

2) The left-hand side flange fracture at t_{f1} is accompanied by an instantaneous fracture of the entire web. The energy release associated with this event induces a local dynamic response at the splice nodes, evident from the "flip-flopping" of the axial force and bending moment in the splice element (See Mark 1 in Figure 12B and 12C). The fracture of the left-hand side flange and the web instantaneously changes the forces through the splice element and the flexural stiffness of the splice element.
3) Between the instants t_{f1} and t_{f2}, the effective stiffness of column AB is markedly diminished (as may be inferred from Figure 11F, which indicates the lateral load versus time response, noting that the time may be considered a proxy for the displacement). This reduced stiffness is attributed to the loss of one flange and the web. The stiffness of column CD, without a splice, is unaffected. Referring to Figure 12B and 12C, the SFE and column AB maintain tensile loads after t_{f1}, and the bending moment in the SFE changes sign with just the right-hand side flange remaining, which is modeled as a single fiber. The tensile stress in the right-hand side flange increases with the applied displacement until it reaches the fracture stress at t_{f2} (see illustration at t= 2.4s in Figure 12E and t=t_{f2} in Figure 12F).
4) At t_{f2}, the right-hand side flange fractures, resulting in the severing of the entire section. The energy release leads to horizontal oscillation of the upper column segment over a very brief period (~0.2 sec), as shown in the illustrations of

the deformed shape of the splice and the portal frame at time instants following t_{f2} in Figure 12F. Minor axial force and bending moment oscillations in the SFE, shown in Mark 2 in Figure 12B and 12C, respectively, during this phase are attributed to the dashpots in the two directions; these prevent unbounded response, as discussed earlier.

5) Between t_{f1} and $t_{contact}$, the upper column segment is disconnected from the lower one at the splice location (see illustration at t= 13.54s in Figure 12F). Although present in the simulation model and under double curvature from a deformation standpoint, the SFE transfers zero axial force, moment, and shear due to the non-local transfer of strains (see Figure 12B). Referring to Figure 11F, the base shear in column AB changes to zero as expected. The stiffness of column CD reduces significantly at t_{f1} (see Figure 11G) as it now acts as a cantilever column with a large overhang. At $t_{contact}$, the stiffness of column CD changes again, suggesting that the splice element captures the contact of the upper column segment with the lower one effectively.
6) At $t_{contact}$, the right-hand side flange of the upper column segment establishes contact with the lower column segment. The impact at this instant is regulated by the vertical and rotational dashpot, evident from the axial force and the bending moment in the splice element shown in marking 3 in Figure 12B and 12C. Beyond this instant, the right-hand side flange fiber acts as a truss element and transfers compressive stresses between the upper and lower column segments, provided that the contact is maintained.
7) After $t_{contact}$, only the right-hand side flange remains in contact with the lower column segment throughout the remaining loading due to the deformed shape with which the upper column segment seats on the lower one. Since the SFE lacks the capability to transfer friction forces at the contact interface, the upper column segment slides on the lower one. The sliding is reflected in the deformed shape of the splice and the portal frame, as shown in Figure 12H when the applied displacement is towards the left-hand side at t = 60s. Referring to Figures 12B, the axial force and moment in the SFE increase, while the shear force remains zero throughout the remaining loading due to the equal strain at the two IPs of all the fibers.
8) At t= 79.99 seconds, when the applied displacement brings the top node to its initial horizontal location, the right-hand side flange loses contact, and the entire upper column segment is disconnected from the lower one.

These detailed observations collectively underscore the performance of the SFE throughout various phases of loading, providing a thorough validation of its efficacy in capturing the behavior of the structural system when splice fracture occurs. To further examine the performance of the SFE, NLRHA simulation of a 20-story steel moment frame is presented in the next section.

5 | APPLICATION TO 20-STORY FRAME

Referring to the previous section, the SFE effectively captures the onset of fracture, the post-fracture response of the splice, and the influence on the global response. This section applies the SFE within a 5-bay, 20-story steel moment frame to (1) further investigate the efficacy of the SFE in full-scale NLRHA simulations and (2) examine the types of global response characteristics, e.g., patterns of splice fracture and force redistribution that may occur in realistic settings and may be simulated by the SFE.

Figure 13A shows the overall frame configuration, which is adapted from the archetype buildings used in the SAC steel project.[39] This similar to the frame used in previous studies for seismic demand characterization and fracture fragility evaluation of the pre-Northridge welded column splices[5–8] without capturing the splice fracture and post-fracture response. The same frame is used by Stillmaker et al.[23] to show the application of the material model to capture splice fracture and post-fracture response with limitations in the frame simulation. The 20-story frame is designed as per ASCE 7–05[40] and AISC 341–10,[41] for seismicity consistent with the Los Angeles area, California with firm soil conditions (Site Class D), and typical gravity loading for office occupancy. It is important to acknowledge that the building is designed as per codes and standards developed after the Northridge earthquake. However, as noted by Gupta and Krawinkler,[39] the frames designed pre and post-Northridge are similar in global response and member forces demands due to the Strong-Column-Weak-Beam consideration introduced after the 1971 San Fernando earthquake. The beam-column connections are provided with Reduced Beam Section (RBS) detailing, which is typical of modern construction. The splice levels in the frame are indicated in Figure 13A using arrows. At each spliced level, splices are located 1.22 m (4 ft.) from the top surfaces of the lower story beams, which is the minimum distance requirement as per AISC 341–10.[41] The splices are considered to be provided with 50% PJP weld and the weld material is considered to have a Charpy impact energy of 13.6 J at 21°C, which

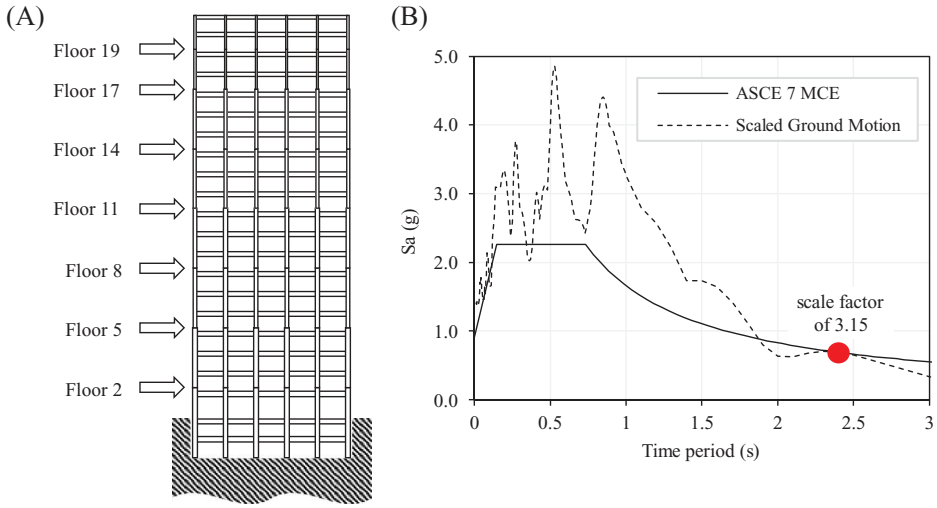

FIGURE 13 (A) 20-story frame, (B) Scaling of pseudo-spectral acceleration at the fundamental period of the building for the ground motion to match the *S_a* values given by the MCE hazard level in Los Angeles, California.

are typical of the pre-Northridge detailing and material[5,20]; this controls the estimation of fracture stress, $\sigma_{fracture}$, in each splice.

The model is developed in OpenSees following the process outlined Stillmaker et al.,[23] with the exception that the SFE is inserted at the splice location. All beam and column elements, including the RBS details, are modeled as force-based fiber elements to simulate the axial-flexure interaction and the spread of plasticity through the member length. A bilinear kinematic hardening material model, *Steel01* in OpenSees, is used to represent the cyclic response of the steel material. The steel material is assigned a yield stress of 380 MPa (corresponding to expected yield strength of A572 Gr. 50 Steel) and a hardening slope of 5% of the elastic modulus ($E = 200$ GPa), consistent with previous studies.[5–8,23] As large displacements are expected after the fracture of splices, corotational geometric transformation is used for all the columns in the model. A rigid diaphragm constraint is imposed. The panel zone flexibility is not explicitly simulated and finite joint size using rigid offsets is modeled. A leaning column is modeled to simulate the destabilizing effect of the vertical loads on gravity frames. The lateral resistance of the gravity frames is however not considered, and it is assumed that the splices in the gravity frames do not fracture. The skeletal nodes are assigned mass based on tributary area of the frame and the top and bottom splice nodes are assigned mass equal to half the weight of the column segment above and below the splice element respectively.

The splices are modeled as SFE, implemented in OpenSees as *dispBeamColumnSplice*. The material model proposed by Stillmaker et al.[23] is assigned to the splices. The bilinear kinematic hardening material model, *Steel01*, with properties same as the beam and column elements, is used as Material C (See Figure 6A). The fracture stress, $\sigma_{fracture}$ of the splices is determined using the framework developed by Jhunjhunwala and Kanvinde[20] and a Lowest Anticipated Service Temperature of 10^0C. The framework provides fracture fragility curves for the splices, incorporating various sources of uncertainty. For this study, the median splice fracture stress, as determined from this framework, is used as a realistic value of $\sigma_{fracture}$. The splices in the 20-story frame have $\sigma_{fracture}$ in the range of $0.3F_y$ to $0.45F_y$. The splice elements are assigned a linear geometric transformation and two integration points as required by the element construct. The flanges are modeled as single fiber in the fiber discretization. Three sets of models are developed for the 20-story frame:

1) A model incorporating the SFE with a median fracture stress capacity, referred to as the *Complete Fracture Model* (CFM).
2) A model without the splice element, referred to as the *No Fracture Model* (NFM). This represents a building where the column splices have been completely retrofitted, ensuring they do not fracture.
3) A model with the splices modeled using standard displacement-based beam-column elements with the material model proposed by Stillmaker et al.[23] The same fracture stress used for the CFM is used in this model. This approach captures the loss of flexural strength associated with splice fracture (i.e., it effectively converts the splice into an internal hinge when all the fibers have zero strength). However, it does not adequately capture the shear loss. This model is referred to as the *Flexure Fracture Model* (FFM).

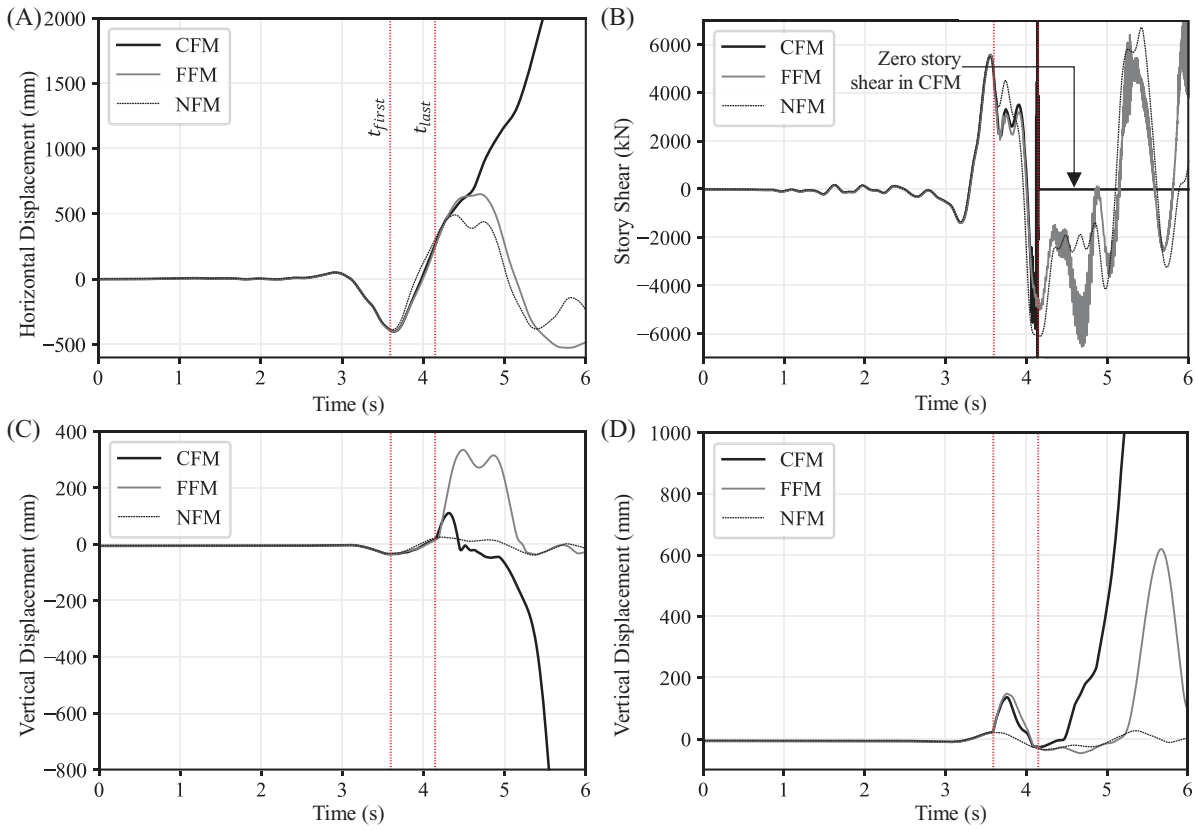

FIGURE 14 Response of 20-story frame subjected to MCE (A) Horizontal displacement of roof nodes, (B) Story shear at 14th Floor (C) Vertical displacement of left-hand side exterior roof node, (D) Vertical displacement of right-hand side exterior roof node.

The models are subjected to a scaled Northridge earthquake record (RSN 953 in the PEER NGA-West2 database[42]). The ground motion has a PGA of 0.44g and a time duration of 30s. The scaling is conducted to match the spectral acceleration, S_a, value at the fundamental period of the structure (determined as 2.36s) with the Maximum Considered Earthquake (MCE) spectral acceleration, which corresponds to a hazard of 2% probability of exceedance in 50 years. Spectral accelerations for MCE are obtained for the Los Angeles region, considering stiff soil conditions, using the ASCE 7 hazard tool (reference). Figure 13B illustrates the scaling of the ground motion to MCE level hazard. The motion and scaling are selected to provide a significant level of shaking that results in the fracture of all the splices.

The response of the three models – CFM, FFM and NFM, to the ground motion scaled to MCE level hazard (referred to as MCE henceforth) is shown in Figure 14. Figure 14A and 14B show the horizontal displacement response of the roof level and the story shear at 14th Floor, respectively. Figure 14C and 14D show the vertical displacement response of the right-hand side and left-hand side exterior nodes at the roof level respectively. The red dotted line marked t_{first}. in the figures corresponds to the time instant when fracture is first observed in any splice in the CFM. The second red dotted line corresponds to the time when all the splices on any given floor are fractured entirely in the CFM, referred to as t_{last}. Figure 15A and 15B illustrate the progression of splice fracture at various instants in the CFM and FFM respectively. The hollow black circles correspond to splices that have not fractured, the hollow red circles correspond to splices that have one of the flanges and the web fractured, and the solid red circles correspond to the splices that have fractured entirely. Referring to these figures, the following observations are made:

1) Referring to Figure 14, the response of the three models is identical before the first fracture. The first fracture in the FFM coincides with that in the CFM, because the splice material is identical in both models. This splice location is illustrated at the instant denoted t_{first} in Figure 15.
2) Referring to Figure 15, the fracture progresses through all the 14th floor splices within a duration of roughly 0.5 seconds, initiating at the right-hand side exterior column splice for both the CFM and the FFM. The difference in t_{last}, i.e., the time at which the last splice on the 14th floor (the left-hand side exterior column splice) fractures in the two models, is less than 0.1 seconds, indicating that the FFM adequately captures the sequence of the first series of fractures.

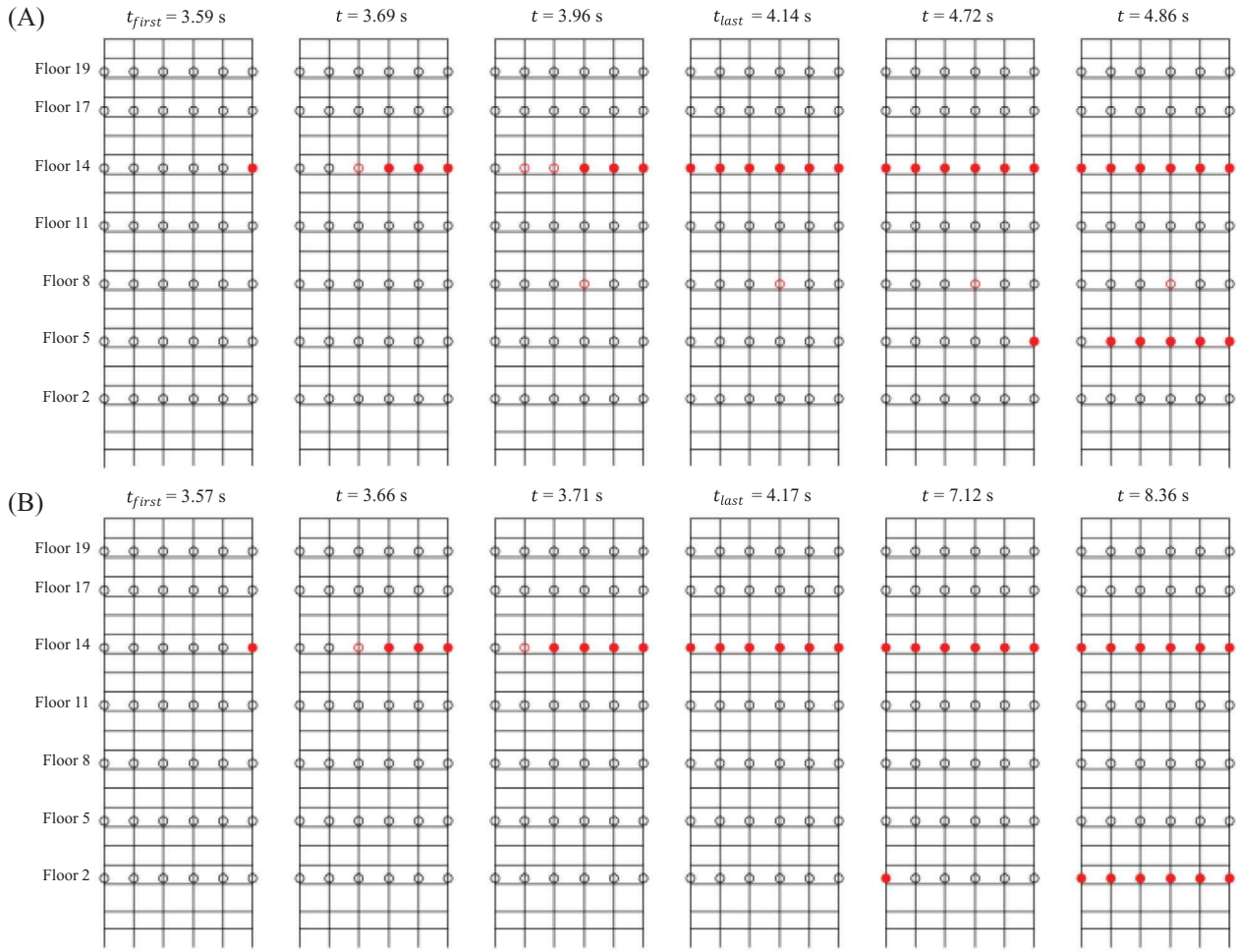

FIGURE 15 Fracture sequence of splices in 20-story frame (A) CFM (B) FFM.

3) Although the FFM captures the sequence of the first series of fractures, the fractured splices in the FFM provide shear connectivity through the splice element, because they are modeled using the standard displacement-based fiber elements. Referring to Figure 14B, the story shear through the 14th floor in FFM is significant and similar to the NFM after t_{last} despite all the splices on the floor being fractured. This is overcome by the SFE. The story shear through the floor in the CFM, where the splices are modeled as the SFE, is zero after t_{last}, reflecting the shear loss in the SFE after fracture.
4) Referring to Figure 14A,C, and, the horizontal displacement of the roof nodes and the vertical displacement of the exterior roof nodes in the CFM is unbounded after t_{last}. This indicates that the portion of the building above the 14th floor is disconnected from the lower portion of the building – which may be considered a suitable indicator of collapse or the end of analysis. On the other hand, the building is held in place in the FFM, where the shear connectivity is maintained in the splices. This highlights the importance of modeling shear loss in these splices.
5) After the fracture of the 14th floor splices in the CFM, splice fractures on the 5th floor immediately follow (see illustrations to the right of t_{last} in Figure 15A). On the contrary, the FFM does not simulate this sequence of fractures due to the shear connectivity in the splice element, and the following sequence of fractures in the FFM occurs on a different floor (2nd floor) after a few seconds (see illustrations to the right of t_{last} in Figure 15B). The ability to capture the sequence of fracture events by the CFM is essential when assessing the progressive collapse of the building.

The NLRHA simulations of the 20-story frame yield interesting observations about the SFE element itself, the frame response, and the role of modeling splice fracture with various degrees of sophistication. By and large, the SFE is shown to successfully represent the key phenomena associated with splice fracture and post-fracture response. Moreover, the SFE shows facile convergence (similar to the FFM and NFM models) until an entire story is severed – this is considered

an acceptable limitation in modern performance assessment frameworks. Regarding the building response, the ability to represent shear loss is essential and results in significantly different performance relative to building models in which such response is not modeled (i.e., FFM and NFM). These differences pertain to the overall structural performance (the CFM predicts an earlier onset of collapse relative to the FFM) and the pattern or sequence of fracture propagation within buildings. Such observations may inform tradeoffs regarding the retrofit/repair of splices and, more specifically, selective retrofit of splices that may offer the highest cost-benefit with respect to structural performance.

6 | SUMMARY, CONCLUSIONS, AND LIMITATIONS

The fracture risk of welded column splices in pre-Northridge steel moment resisting frames has been a focus of recent studies, given its implications for public safety and the resilience of these buildings. The problem has multiple aspects, ranging from estimating the fracture risk of individual splices to assessing the overall performance of building frames within which these splices are present. For the latter, a favored approach is to consider the fracture of any splice as the end of the building response. While conservative from a safety standpoint, this approach disregards the response of the building after splice fracture and the associated force redistribution within the frame. While this approach inhibits true physics-based performance assessment, it is favored mainly due to the lack of alternative simulation approaches that are able to capture the full range of phenomena associated with splice fracture.

Within this professional setting, a new Splice Fracture Element (SFE) is presented, which overcomes many of the limitations of previous modeling approaches. The element is a 2-dimensional beam-column fiber element that may be inserted at the locations of column splices. The element contains the following features: (1) a constitutive material model that represents the loss of strength of individual fibers when critical fracture stress is reached, (2) a non-local modification to represent shear loss when the entire section is severed, and (3) tracking of section kinematics to represent the response associated with contact after fracture. The formulation is implemented as a new element *dispBeamColumnSplice* in the OpenSees platform. Two demonstrative exercises are presented in this paper. The first involves the application of the SFE to a one-story, one-bay frame, providing the opportunity for a close-in examination of SFE element response and its interaction with global structural response. The results of this analysis are promising, indicating that the SFE is able to capture all forms of response that it is designed to, including fracture, shear-loss, and contact behavior. The second application involves a 5-bay, 20-story moment frame subjected to NLRHA under a high-intensity ground motion. The results of this simulation indicate that the SFE is ready for use in full-scale structural simulation and simulates important aspects of splice fracture and post-fracture response with efficacy. The results are compared to benchmark NLRHA, which does not simulate splice fracture or simulate only the loss of flexural strength. The comparison indicates the importance of representing all aspects of splice fracture response, particularly the loss of shear capacity. In summary, the new SFE element offers promise for use within NLRHA simulations, overcoming the limitations of existing simulation tools and ultimately resulting in improved performance assessment.

The absence of experimental validation for the proposed approach bears some additional discussion. In this regard, it is observed that shake table studies with fracturing columns or column splices that are ideally required for validation are not readily available. Nonetheless, other observations provide support for the approach, and the underlying assumptions. First, from a purely phenomenological standpoint, the SFE captures all intended aspects of response – confirming the ability to functionally represent splice fracture, although experimental data will provide the opportunity for refinement, e.g., introduction of frictional response. Second, shake table tests with fracturing beams[25] show strain spikes and dynamic behavior similar to that predicted by the proposed approach, albeit without shear-loss. Finally, the SFE formulation assumes brittle fracture wherein the entire flange fractures simultaneously and instantly. This is supported by experimental data,[6] as well as fracture-mechanics; specifically:

1. The splices tested Shaw et al.[6] featured notch-tough weld material as well as flaw sizes that were significantly lower than in pre-Northridge splices. Despite these favorable characteristics, the experimental splices fractured catastrophically in a brittle way, even under quasi-static loading. This supports the assumption of brittle fracture for pre-Northridge splices.
2. From a fracture mechanics standpoint, the seismic load rate may be considered "slow" relative to crack propagation speeds. This implies force-controlled loading, wherein (due to material damping and inertial effects) the remote stresses do not reduce as the crack grows. Under such loading, the fracture toughness demand increases with the crack length.[43] On the other hand, when fracture is controlled by brittle mechanisms, the fracture toughness capacity does not increase

correspondingly (i.e., a flat resistance curve is noted[43]). This results in an instability and nearly instantaneous fracture of the entire flange.

While promising, the proposed element has limitations that must be considered in its use and in the interpretation of NLRHA results obtained using it. First, the element is a 2-dimensional element, which cannot address 3-dimensional response and biaxial bending of the columns, which is often critical. Second, the element relies on the use of critical fracture stress, determined independently, thereby inheriting the limitations of the approaches[13,20,21] used to estimate it, which are numerous (e.g., the disregard of loading history effects, residual stresses – see Jhunjhunwala and Kanvinde[20] for details). With regards to the element formulation itself, the key limitations pertain to the following: (1) the disregard of shear stresses in estimating failure – e.g., full shear connectivity is maintained even if a small part of the section remains attached, (2) shear transfer due to friction after reseating is not considered, and (3) contact response idealizes the fibers as truss-like elements, an assumption that is driven by expediency. These limitations arise from the desire to maintain a degree of simplicity and convenience in the formulation while still capturing important aspects of the response. Future work, including experimental validation of the developed element, may guide further development and enhancements to the framework.

ACKNOWLEDGEMENTS

The authors are grateful to the Pacific Earthquake Engineering Research Center, University of California Berkeley (Grant No. 1158-NCTRVI) and the National Science Foundation (Grant No. 2129445) for their support. The findings presented in this paper do not reflect those of the sponsors and are solely those of the authors.

DATA AVAILABILITY STATEMENT

Some or all data, models, or code that support the findings of this study are available from the corresponding author upon reasonable request.

ORCID


Aditya Jhunjhunwala https://orcid.org/0000-0001-5408-1035

REFERENCES

1. Fuller T, Singhvi A, Williams J. San Francisco's Big Seismic Gamble. The New York Times. 2018. Accessed May 6, 2024. https://www.nytimes.com/interactive/2018/04/17/us/san-francisco-earthquake-seismic-gamble.html
2. SAC Joint Venture. *Analytical and Field Investigations of Buildings Affected by the Northridge Earthquake of January 17, 1994*. Federal Emergency Management Agency; 1995.
3. SAC Joint Venture. *Technical Report: Case Studies of Steel Moment-Frame Building Performance in the Northridge Earthquake of January 17, 1994*. Federal Emergency Management Agency; 1995.
4. AISC. *Seismic Provisions for Structural Steel Buildings*. American Institute of Steel Construction; 2016.
5. Galasso C, Stillmaker K, Eltit C, Kanvinde A. Probabilistic demand and fragility assessment of welded column splices in steel moment frames. *Earthquake Eng Struct Dynam*. 2015;44(11):1823-1840. doi:10.1002/eqe.2557
6. Shaw SM, Stillmaker K, Kanvinde AM. Seismic response of partial-joint-penetration welded column splices in moment-resisting frames. *Eng J*. 2015;52(2):87-108.
7. Shen J, Sabol TA, Akbas B, Sutchiewcharn N, Cai W. Seismic demand on column splices in steel moment frames. *Eng J*. 2010;47(4):223.
8. Song B, Galasso C, Kanvinde A. Advancing fracture fragility assessment of pre-Northridge welded column splices. *Earthquake Eng Struct Dynam*. 2020;49(2):132-154. doi:10.1002/eqe.3228
9. Nudel A, Dana M, Maclise L. Adaptive Reuse: Creating a New School of Dentistry in an Outdated Urban Office Building. In: *SEAOC 2013 Convention Proceedings*; 2013:63-74.
10. Fisher J, Dexter R, Kaufmann E. Fracture mechanics of welded structural steel connections. In: *Background Reports: Metallurgy, Fracture Mechanics, Welding, Moment Connections and Frame Systems Behavior*. Technical Rep. 95-09. SAC Joint Venture; 1995.
11. Kaufmann EJ, Fisher JW, Di Julio RM, Gross JL. *Failure Analysis of Welded Steel Moment Frames Damaged in the Northridge Earthquake*. National Institute of Standards and Technology; 1997.
12. Kaufmann EJ, Xue M, Lu LW, Fisher JW. Achieving ductile behavior of moment connections. *Modern Steel Construction*. 1996;36(1):30-39.
13. Stillmaker K, Kanvinde A, Galasso C. Fracture Mechanics-Based Design of Column Splices with Partial Joint Penetration Welds. *J Struct Eng*. 2016;142(2):04015115. doi:10.1061/(ASCE)ST.1943-541X.0001380
14. SAC Joint Venture. *Recommended Seismic Design Criteria for New Steel Moment-Frame Buildings*. Federal Emergency Management Agency; 2000.
15. SAC Joint Venture. *Recommended Seismic Evaluation and Upgrade Criteria for Existing Welded Steel Moment-Frame Buildings*. Federal Emergency Management Agency; 2000.

16. Hamburger RO. Prequalified moment connections. *Modern Steel Construction*. 2014;54(3):70-72.
17. AIJ. *Reconnaissance Report on Damage to Steel Building Structures Observed from the 1995 Hyogoken-Nanbu (Hanshin/Awaji) Earthquake*. Steel Committee of Kinki Branch, The Architectural Institute of Japan; 1995.
18. Chisholm MP, Pekelnicky RG, Malley JO. High-Rise Pre-Northridge Partial Joint Penetration Column Splice Repair. In: *SEAOC 2017 Convention Proceedings*; 2017.
19. Applied Technology Council. *Research Plan for the Study of Pre-Northridge Earthquake Weak Panel Zones and Welded Column Splices with PJP Groove Welds*. National Institute of Standards and Technology; 2022. doi:https://www.atcouncil.org/atc-153
20. Jhunjhunwala A, Kanvinde A. Fracture Mechanics–Based Fragility Assessment of Pre-Northridge Welded Column Splices. *J Struct Eng*. 2023;149(6):04023062. doi:10.1061/JSENDH.STENG-11749
21. Applied Technology Council. *Guidelines for Nonlinear Structural Analysis for Design of Buildings: Part IIa – Steel Moment Frames*. National Institute of Standards and Technology; 2017.
22. Bruneau M, Mahin SA. Ultimate Behavior of Heavy Steel Section Welded Splices and Design Implications. *J Struct Eng*. 1990;116(8):2214-2235. doi:10.1061/(ASCE)0733-9445(1990)116:8(2214)
23. Stillmaker K, Lao X, Galasso C, Kanvinde A. Column splice fracture effects on the seismic performance of steel moment frames. *J Constr Steel Res*. 2017;137:93-101. doi:10.1016/j.jcsr.2017.06.013
24. McKenna F, Fenves G, Scott M. Open system for earthquake engineering simulation (OpenSees). Published online 2018.
25. Rodgers JE, Mahin SA. Local fracture-induced phenomena in steel moment frames. *Earthquake Eng Struct Dynam*. 2009;38(2):135-155. doi:10.1002/eqe.839
26. Spacone E, Filippou FC, Taucer FF. Fibre Beam–Column Model for Non-Linear Analysis of R/C Frames: Part I. Formulation. *Earthquake Eng Struct Dynam*. 1996;25(7):711-725.
27. Hsiao PC, Lehman DE, Roeder CW. A model to simulate special concentrically braced frames beyond brace fracture. *Earthquake Eng Struct Dynam*. 2013;42(2):183-200. doi:10.1002/eqe.2202
28. Galvis FA, Deierlein GG, Hutt CM, Baker JW. High-fidelity modeling of fracture-critical welded steel beam-to-column connections and their impact on earthquake stability of tall buildings. In: *Proceedings of the Annual Stability Conference Structural Stability Research Council*, Denver, Colorado; 2022.
29. Clough RW, Johnston S. Effect of stiffness degradation on earthquake ductility requirements. In: *Proceedings of Japan Earthquake Engineering Symposium*; 1966.
30. Elwood KJ. Modelling failures in existing reinforced concrete columns. *Can J Civ Eng*. 2004;31(5):846-859.
31. Vulcano A, Bertero VV, Colotti V, others. Analytical modeling of RC structural walls. In: *Proceedings of the 9th World Conference on Earthquake Engineering*. Vol 6.; 1988:41-46.
32. Kolozvari K, Orakcal K, Wallace JW. Modeling of Cyclic Shear-Flexure Interaction in Reinforced Concrete Structural Walls. I: Theory. *J Struct Eng*. 2015;141(5):04014135. doi:10.1061/(ASCE)ST.1943-541X.0001059
33. Talaat M, Mosalam KM. Modeling progressive collapse in reinforced concrete buildings using direct element removal. *Earthquake Eng Struct Dynam*. 2009;38(5):609-634. doi:10.1002/eqe.898
34. Neuenhofer A, Filippou FC. Evaluation of Nonlinear Frame Finite-Element Models. *J Struct Eng*. 1997;123(7):958-966. doi:10.1061/(ASCE)0733-9445(1997)123:7(958)
35. De Borst R, Crisfield MA, Remmers JJ, Verhoosel CV. *Nonlinear Finite Element Analysis of Solids and Structures*. John Wiley & Sons; 2012.
36. Kolwankar S, Kanvinde A, Kenawy M, Kunnath S. Uniaxial Nonlocal Formulation for Geometric Nonlinearity–Induced Necking and Buckling Localization in a Steel Bar. *J Struct Eng*. 2017;143(9):04017091. doi:10.1061/(ASCE)ST.1943-541X.0001827
37. Wu S, Wang X. Mesh Dependence and Nonlocal Regularization of One-Dimensional Strain Softening Plasticity. *J Eng Mech*. 2010;136(11):1354-1365. doi:10.1061/(ASCE)EM.1943-7889.0000184
38. Hamitouche L, Tarfaoui M, Vautrin A. An interface debonding law subject to viscous regularization for avoiding instability: Application to the delamination problems. *Eng Fract Mech*. 2008;75(10):3084-3100. doi:10.1016/j.engfracmech.2007.12.014
39. Gupta A, Krawinkler H. *Prediction of Seismic Demands for SMRFs with Ductile Connections and Elements, SAC Steel Project Background Document*. SAC Joint Venture; 1999.
40. *ASCE*. Minimum Design Loads for Buildings and Other Structures. ASCE/SEI-7. American Society of Civil Engineers; 2005.
41. AISC. *Seismic Provisions for Structural Steel Buildings*. American Institute of Steel Construction; 2010.
42. Ancheta TD, Darragh RB, Stewart JP, et al. *PEER NGA-West2 Database*. Pacific Earthquake Engineering Research Center, University of California, Berkeley; 2013. https://peer.berkeley.edu/sites/default/files/2013_03_ancheta_7.3.2020.pdf
43. Anderson TL. *Fracture Mechanics: Fundamentals and Applications*. CRC press; 2017.

How to cite this article: Jhunjhunwala A, Maity A, Kanvinde A. Simulating column splice fracture and post-fracture response for seismic assessment of steel moment frames. *Earthquake Engng Struct Dyn*. 2024;1-24. https://doi.org/10.1002/eqe.4248